Major explosive activity in the Monti Sabatini Volcanic District (central Italy) over the 800-390 ka interval: geochronological - geochemical overview and tephrostratigraphic implications

Marra, F.[(1)], Sottili, G.[(2)], Gaeta, M.[(3)], Giaccio, B.[(2)], Jicha, B.[(4)], Masotta, M.[(3)], Palladino D.M.[(3)], Deocampo, D.M.[(5)]

1) Istituto Nazionale di Geofisica e Vulcanologia - Rome - Italy
2) Istituto di Geologia Ambientale e Geoingegneria, CNR - Montelibretti, Rome - Italy
3) Dipartimento di Scienze della Terra, Sapienza-Università di Roma, Rome - Italy
4) Department of Geoscience University of Wisconsin - Madison - USA
5) Department of Geosciences, Georgia State University - Atlanta - USA

Corresponding author:
Fabrizio Marra
Istituto Nazionale di Geofisica e Vulcanologia
Via di Vigna Murata 605 - 00147 - Rome, Italy
e-mail: fabrizio.marra@ingv.it
phone: +39 0651860420
fax: +39 0651860507

Abstract

A review of the existing chronological, stratigraphic and chemo-petrologic data of the major eruptive units from the early phase of activity (800-390 ka) in the Monti Sabatini Volcanic District (MSVD), belonging to the ultra-potassic magmatic region of central Italy, is presented along with new radioisotopic age determinations and geochemical analyses. Through the combined use of electron microprobe glass compositions, selected trace-element compositions, and single-crystal $^{40}Ar/^{39}Ar$ age determinations, we provide a new chrono- and chemo-stratigraphic classification of the products emplaced in the 800-390 ka time interval. Besides giving insights on the petrologic evolution of the Roman Comagmatic Region, the large dataset provides fundamental information that is applicable to tephrostratigraphic studies in the wide region encompassing the Tyrrhenian Sea margin to the Adriatic Sea basin. Distal tephras from this volcanic activity also act as important geochronologic markers for the coastal sedimentary successions deposited in response to glacio-eustatic fluctuations, as well as for successions in the Quaternary tectonic basins of the Central and Southern Apennines. An innovative approach based on the use of discrimination diagrams of Zr/Y vs Nb/Y ratios for fingerprinting altered volcanic rocks - recently developed and successfully employed in archaeometric studies - is here combined to the glass compositions for classifying the MSVD deposits and tested on two distal tephra layers, showing its potentiality for tephrostratigraphic correlation.

Key-words: **Monti Sabatini Volcanic District, high-K magmatism, geochronology, geochemistry, tephrostratigraphy, central Italy**

1. Introduction

The recognition of distal tephra layers deposited in sedimentary successions and their correlation with proximal pyroclastic units are an important stratigraphic method. Tephrostratigraphy is in fact a pinpoint tool for a number of geological, paleoenvironmental and archaeological topics, providing a reliable control of the chronological framework (e.g. Lowe et al., 2011). The applicability and reliability of tephrostratigraphy are, however, subordinated to the depth of knowledge of the stratigraphy, chronology, petrology and major element glass and isotopic compositions of the proximal pyroclastic units. Indeed, without a reliable and robust reference dataset, tephrostratigraphy become an useless or even misleading chrono-stratigraphic tool.

The peri-Tyrrhenian high-K magmatic region, developed during the Pleistocene on the Tyrrhenian Sea margin of Central Italy (Peccerillo, 2005, and references therein), represents an important source of tephras due to the occurrence of intense explosive activity. However, with the exception of few notable cases of study (e.g., Colli Albani Volcanic District; Giaccio et al., 2013a), the lack of diagnostic data on proximal pyroclastic units limits most of these potential tephra sources for distal tephrostratigraphic purposes. This is particularly true for the Monti Sabatini Volcanic District (MSVD), whose eruptive history was dominated by frequent, highly explosive events up to at least 90 ka (e.g. Sottili et al., 2004, 2010). The mid-distal occurrences of the tephras from this volcanic activity provide important geochronological constraints for the coastal sedimentary successions deposited in response to glacio-eustatic fluctuations, like the Paleo-Tiber aggradational sections, which serve as an independent calibration of the oxygen isotope curves (Karner and Renne, 1998; Karner and Marra, 1998; Marra et al., 1998; Florindo et al., 2007; Marra et al., 2008). However, when dealing with very distal sedimentary successions, the correlation of given tephras to individual MSVD units is hardly tenable and often the correlation is, even if plausible, only hypothetic (e.g., Karner et al., 1999; Munno et al., 2001; Galli et al., 2010; Giaccio et al., 2013b).

In order to strengthen the potential use of the MSVD tephras for tephrostratigraphic purposes, in the present work we have combined field, geochronological and geochemical investigations to provide

a detailed chrono- and chemo-stratigraphic framework of the main phase of activity spanning the 589-389 ka interval, integrating, and in some instances revising, the previous outline. Specifically, here we integrated the existing data (Conticelli et al., 1997; Sottili et al., 2004; Masotta et al., 2010, Galli et al., 2010; Marra et al., 2012; Marra et al., 2011; Lancaster et al., 2010) with new detailed chemo-chronostratigraphic investigations by bulk rock and electron microprobe (EMP) analyses, and $^{40}Ar/^{39}Ar$ age determinations. Following a recently developed methodology (Marra et al., 2011, 2012; Marra and D'Ambrosio, 2012), we also propose a classification of the altered MSVD mid-distal deposits by combining selected trace-element diagrams (i.e.: Zr/Y vs Nb/Y) with major element analysis, thus providing diagnostic criteria for establishing tephrostratigraphic correlations. In particular, we provide two case-histories by testing this method on two distal tephra layers collected in the Sulmona and in the Mercure lacustrine basins, occurring in the central and southern Apennines.

2. Stratigraphic setting

The MSVD is part of the Roman Comagmatic Province (Peccerillo, 2005, and references therein), a high-K magmatic region that developed during Pleistocene times on the Tyrrhenian Sea margin of Central Italy. The MSVD activity was characterized by K-rich magma composition, feeding dominant explosive eruptions ranging from hydromagmatic to Plinian and large pyroclastic flow forming events (VEI up to 4-5; Sottili et al., 2004), with erupted magma up to 10 km^3 for individual events, and subordinate effusive episodes.

The subject of the present paper is the MSVD ancient explosive activity, localized at the two source areas of Morlupo and Southern Sabatini. The climactic phases of this activity period spanned the interval 800-390 ka and are separated by a >100 kyr-long, relative dormancy, from the following period occurring at the Bracciano and Sacrofano source areas (315 ka; Sottili et al., 2010). A late

hydromagmatic phase, characterized by several monogenetic centers, occurred between 150 and 90 ka and represents the most recent volcanic phase in the MSVD (Sottili et al., 2010).

The oldest products attributed to the MSVD activity are represented by several tephra layers, sporadically intercalated within late Lower-early Middle Pleistocene fluvial deposits of the Paleo-Tiber River, dated between 802±6 ka and 605±11 ka[1] (Karner & Renne, 1998; Marra et al., 1998; Karner et al., 2001; Florindo et al., 2007). The vent area of these products is uncertain. A more continuous, extensive explosive phase of activity is documented by a thick succession of pyroclastic-flow and fallout deposits that constitute the Vulcani Sabatini Products (Scherillo, 1947; Mattias and Ventriglia, 1970: geologic map 1:100.000), cropping out above the Plio-Pleistocene sedimentary substrate over a ca. 1,500 km^2 area to the NW of Rome (Figure 1). The early Plinian-style eruptions, emplacing fall levels and accretionary lapilli-rich ash layers (*Pyroclastic fall products from the Morlupo edifice,* de Rita et al., 1983; 1993), as well as a spatter-flow deposit (*Morlupo trachyte*, dated at 587±4 ka; Cioni et al., 1993), whose stratigraphic relationship with respect to the other explosive products is unclear, have been attributed by de Rita et al. (1983) to the activity of the Morlupo center (Figure 1). Subsequent explosive activity, responsible for the emplacement of the "Sacrofano lower pyroclastic flow unit" of de Rita et al., 1993 (corresponding to the "Tufo Giallo della Via Tiberina" of Mattias and Ventriglia, 1970; Alvarez, 1972; 1973; Nappi et al., 1979), was instead attributed to the activity of the volcanic center of Sacrofano (Figure 1).

A first comprehensive geochronological framework and a revision of the stratigraphy for the MSVD were provided in Karner et al. (2001). Besides verifying an age of 582±2 ka for the earliest fallout deposit (First Ashfall Deposits), these authors recognized a series of large pyroclastic-flow deposits erupted between 561±2 and 514±6 ka (Lower and Upper Tufo Giallo della Via Tiberina, Tufo Giallo di Prima Porta, Grottarossa Pyroclastic Sequence), that were previously grouped with the "Tufo Giallo della Via Tiberina" and the "Tufi stratificati varicolori di Sacrofano" (Mattias and

[1] $^{40}Ar/^{39}Ar$ mean weighted ages in this section are reported as they appear in the original publication. All ages are reported with 2σ analytical uncertainties.

Ventriglia, 1970). Moreover, Karner et al. (2001) introduced the "Tufi Terrosi con Pomici Bianche" pumice and scoria fall succession (488±4 ka), which was investigated in detail by Sottili et al. (2004), who identified 3 major fallout horizons (Fall A, B and C) and attributed them, on the basis of the isopach and isopleth maps, to the Southern Sabatini volcanic center (Figure 1). In the same way, based on the dispersal area of its basal fallout (Fall D, Sottili et al., 2004), also the large pyroclastic-flow forming eruption of the Tufo Rosso a Scorie Nere sabatino (Scherillo, 1940; Alvarez et al., 1975), dated at 449±2 ka (Karner et al., 2001; Cioni et al., 1993), was attributed to this volcanic center. The late activity of the investigated volcanic period is represented by a succession of pumice and scoria fall deposits ("Tufi stratificati varicolori de La Storta", Mattias and Ventriglia, 1970; Corda et al., 1978) that underlie the Tufo Giallo di Sacrofano ("Sacrofano upper pyroclastic flow unit", de Rita et al., 1993) dated at 285±2 ka (Karner et al., 2001). No direct geochronological constraint has been achieved so far for this pyroclastic succession, with the exception of two interbedded pumice fall layers, dated at 416±12 and 410±2 (Bedded Pumice, Karner et al., 2001), both identified in the present work as the Vico α fallout deposit (419±3 ka, Laurenzi and Villa, 1987), from Vico volcano (Figure 1). The lack of significant outcropping of deposits above and below the Vico fallout layers, corroborated by the occurrence of a thick paleosol documented by the present work on top of the 389±4 ka San Abbondio ash-fall succession, suggests that a significant dormancy characterized the MSVD till ca. 315 ka, when a new intense explosive phase of volcanic activity took place, causing the emplacement of the Tufo di Bracciano (316±6 ka) and the Tufo Giallo di Sacrofano (286±6 ka) major pyroclastic-flow deposits (Sottili et al., 2010).

3. Methods

3.1 Field investigations

Field investigations were carried out in the whole Monti Sabatini area (Fig. 1) to obtain an updated and comprehensive stratigraphic framework. A detailed description of the newly recognized

depositional units is provided along with the revisions of the stratigraphic units already described, for which we adopt the chronology and stratigraphic nomenclature outlined in Karner et al. (2001) and Sottili et al. (2004). The readers are thus addressed to these works for the detailed stratigraphy and correlation therein reported.

The reference stratigraphic column showing the geochronologically distinct eruptive events and their relationship with the mid-distal deposits intercalated within fluvio-lacustrine deposits is shown in Figure 2, whereas a historical stratigraphic and geochronologic framework displaying correlation with previous literature is illustrated in Table 1.

3.2 Geochronology

Eight new $^{40}Ar/^{39}Ar$ age determinations presented in this paper and three previously published (Marra et al., 2011) (Table 2) were performed at the University of Wisconsin-Madison Rare Gas Geochronology Laboratory. Sanidine samples and standards were fused using a 25 W CO_2 laser following the methods of Smith et al. (2008). All analyses are single crystal fusions except for samples FAD-3 and TGCP-3, which were 3 and 4 crystal fusions, respectively. Ages are reported with 2σ analytical uncertainties (Table 2; Appendix 1) and are calculated relative to a Fish Canyon Tuff sanidine standard age of 28.201 ± 0.046 Ma (Kuiper et al., 2008) and a value for $\lambda^{40}K$ of 5.463 ± 0.107 x 10^{-10} yr^{-1} (Min et al., 2000). Full $^{40}Ar/^{39}Ar$ data for these experiments are reported in Appendix 1.

We also provide previously unpublished $^{40}Ar/^{39}Ar$ ages of two samples determined at the Berkeley Geochronology Center (Table 3, Appendix 2). Finally, we have reviewed and re-calculated according to the age of 28.201 Ma for the Fish Canyon Tuff sanidine standard (Kuiper et al., 2008) the ages of 34 samples previously dated at the Berkeley Geochronology Center following procedures described in Karner and Renne (1998) (Table 3). In light of the new and re-calculated data, we provide a revised interpretation for the previously published ages of four samples (R93-

25A, R94-30C, Karner and Renne, 1998, GSA data repository item 9845, and SAX-01, PAL-01, Karner et al. 2001; Table 3; full $^{40}Ar/^{39}Ar$ data in Appendix 3).

In the following text, except when expressly stated, all these ages are reported according to the new age of the standard, with 2σ uncertainties.

3.3 Geochemistry

EMP analyses of matrix glass

Electron microprobe (EMP) analyses (Table 4, Appendix 4) were performed on glass from twenty two pyroclastic units at the CNR-IGAG laboratory at Sapienza-University of Rome using a Cameca SX50 EDS-WDS and at Istituto Nazionale di Geofisica e Vulcanologia (Rome, Italy) with a Jeol-JXA8200 EDS–WDS combined electron microprobes. Both instruments are equipped with five wavelength-dispersive spectrometers, using 15 kV accelerating voltage, 10 nA beam current, 2 μm beam size and counting time of 10 and 20 s were used on background and peaks, respectively. The following standards were adopted for the various chemical elements: jadeite (Si and Na), corundum (Al), forsterite (Mg), andradite (Fe), rutile (Ti), orthoclase (K), barite (Ba), celestine (Sr), F-phlogopite (F), apatite (P), spessartine (Mn) and metals (Cr). ZAF correction was used to achieve true element concentrations. The relative analytical uncertainty in the measurements is <1.0%.

XRF analyses

Seven whole rock analyses (Table 5) of selected pumice and scoria clasts were performed at the Dipartimento di Scienze della Terra of the Università di Perugia, using a Philips PW 1400 X-ray fluorescence spectrometer (XRF). The correction for matrix effects was applied following Franzini et al. (1972) and Kaye (1965). The precision is better than 15% for V, Cr, Ni, better than 10% for Co, Cr, Y, Zr, Ba, and better than 5% for all the other elements. The accuracy was verified with international standards and is better than ±10%. FeO, Na_2O and MgO contents and LOI (loss on

ignition) were determined through wet chemical analyses by atomic absorption spectrophotometry, using DR-N, NIM-G, GSN, GA, BCR-1, NIM-l international standards.

FUS-ICP-MS analyses

Forty-nine bulk samples of selected juvenile scoria and pumice (Appendix 5) were analyzed by Lithium Metaborate/Tetraborate Fusion ICP-MS at Activation Laboratories, Ancaster, Ontario, Canada. Fused sample is diluted and analyzed by Perkin Elmer Sciex ELAN 6000, 6100 or 9000 ICP/MS. Three blanks and five controls (three before sample group and two after) are analyzed per group of samples. Wet chemical techniques were used to measure the loss on ignition (LOI) at 900°C. International rock standards have been used for calibration and the precision is better than 5% for Rb and Sr, 10% for Ni, Zr, Nb, Ba, Ce, and La, and 15% for the other elements.

3.4 Zr/Y vs Nb/Y discriminating diagram

Glass chemistry represents an attested method of magma classification, but can be applied only on unaltered products. To overcome these difficulties and attempt correlation among all the investigated products, we have used a trace-element based discrimination method that has been recently developed and successfully applied to geo-archaeological studies (Marra et al., 2011, 2012; Marra and D'Ambrosio, 2012), which relies on ratios of immobile elements that are relatively insensitive to alteration process like Zr, Y and Nb (Cann, 1970; Pearce and Cann, 1973; Floyd and Winchester, 1975; Pearce, 1996). The abovementioned works show that there is no substantial overlapping among the Zr/Y vs Nb/Y compositional fields of the pyroclastic products of Campania and those of Latium and Roccamonfina (see Figure 3a). Limited overlap occurs among the products of the different Latium districts of Vulsini, Vico, Monti Sabatini, and the Colli Albani, allowing in most instances to identify the source area, and in several cases to identify a specific eruption unit from its Zr/Y vs Nb/Y composition (Marra and D'Ambrosio, 2012).

Here, we test the relationships between the distributions in the Zr/Y vs Nb/Y and in the total alkali-silica (TAS) diagrams for all those products of the MSVD for which we obtained both acceptable major element (either obtained by EMP on glass or by XRF and FUS-ICP-MS with LOI<6%) and trace element analyses. Once these relationships are established, we will use the Zr/Y vs Nb/Y diagram to classify those products for which reliable major element analyses are not available, like the most altered distal tephras of the paleo-activity (Figure 3b). In comparing compositions of bulk proximal and distal deposits, however, a possible variation due to the different degree of porfiricity may occur and should be taken into account.

4. Results and discussion

4.1 General compositional features

Figure 4a shows the glass compositions in the total alkali vs silica (TAS) diagram for all samples analyzed by EMP in this and previous studies (Masotta et al., 2010; Sottili et al., 2004), which are representative of the whole activity period of the Morlupo and Southern Sabatini centers (Table 4). Values reported in Figure 4b are the average composition of each individual sample; the complete range of analytical compositions for the samples analyzed in the present work is provided in Appendix 4. Glass compositions are essentially clustered within the trachytic-phonolitic field (MS-A1 field in Figure 4b) with a minority of samples plotting in the tephriphonolitic-latitic field (MS-A2) and in the phono-tephritic field (MS-B; i.e. Grottarossa Pyroclastic Sequence and Fall F). The less differentiated compositions correspond to samples of poorly vesicular, grey scoria (black symbols), in contrast to the trachy-phonolitic compositions of the highly vesicular, white pumice samples (white symbols). The co-existence of whitish, pumiceous, and dark grey, scoriaceous, juvenile clasts is indeed a common feature of most of the MSVD eruptive units (e.g. Sottili et al., 2004; Masotta et al., 2010).

When the distribution in the Zr/Y vs Nb/Y diagram of the homologous samples (Figure 4c) is compared to that in the TAS diagram, a strict correspondence with the compositional fields described above can be established. Most of the analyzed samples plot within a rectangular area in the Zr/Y vs Nb/Y diagram, corresponding to the principal trachyphonolitic compositional field in the TAS diagram (MS-A in Figure 4b, c). A minority of samples displays an offset distribution (MS-B field, bordered by the open dashed line in Figure 4c), corresponding to that defined by the less differentiated samples in the TAS diagram.

Consistent with previous observations in Marra et al. (2011, 2012), the distribution of the samples in the Zr/Y vs Nb/Y diagram reflects that in the TAS diagram, with the higher degree of apparent evolution corresponding to the greater distance from the origin of the axes (arrow a in Figure 4b, c), like it is observed for the two compositional sub-groups MS-A2 and MS-A1. Indeed, the distribution coefficients of Zr and Nb for ultrapotassic magmas are similar and up to one order of magnitude smaller than that of Y (e.g.: Pearce and Norry, 1979). Therefore, while the Zr/Nb is slightly affected by fractional crystallization during the differentiation process, leaving the inclination of the trend substantially constant, Zr/Y and Nb/Y increase in a rather homogeneous measure, and the compositions plot farther and farther away from the origin of the axes. Moreover, a slightly higher compatibility of Zr with respect to Nb, in particular in Al-rich clinopyroxene (Foley and Jenner, 2004), explains another apparent differentiation trend represented by the clockwise rotation of the compositional fields in the Zr/Y vs Nb/Y diagram (arrow a'), which also corresponds to increasing differentiation.

4.2 Stratigraphy and geochronology

The new $^{40}Ar/^{39}Ar$ data and the petro-stratigraphic investigations integrate the previous literature data and allow us to recognize sixteen stratigraphically and geochronologically distinct eruptive events (informally referred to as "eruptive units") occurred in the MSVD in the study period. In

some cases, closely spaced eruptive events, also sharing analogous deposit features and source area, have been grouped in eruption cycles (Figure 2; table 1), as described below. Instead, the fallout deposits spanning 427±5 - 412±5 ka and previously attributed to the MSVD (Bedded Pumice, Karner et al., 2001, are correlated to the activity of the nearby Vico district (Figure 2, Table 1).

4.2.1 Paleo-activity (808±6 - 614±3 ka)

The evidence of this volcanic phase is represented by ten dated tephra layers out of a dozen occasionally exposed in outcrops or recovered from boreholes within fluvio-lacustrine deposits of the Paleo-Tiber River correlated to marine isotopic stages 19, 17 and 15 (Marra et al., 2008, and references therein). Based on radioisotopic age, trace element signature and stratigraphic relationships, we have identified seven distinct eruptive units, and we have grouped the earliest four into a single eruptive cycle (Paleotiber succession; Figure 2 and 3b). Ages for these eruptions are assessed by combining ages of the samples attributed to the same units (Table 6). In order to make correlations among these volcanic layers we had to rely on their trace-element signature, following criteria described in item #1 of the supplementary material, because they are not suitable for EMP glass analysis due to their high degree of alteration. Figure 3b shows the Zr/Y vs Nb/Y compositions of the products of the Paleo-activity. Most samples plot within or at the margin of the principal MSVD field defined by all the bulk samples of the successive phases of activity (MS-A' in Figure 3a; Marra et al., 2011; 2012; Marra and D'Ambrosio, 2012). Moreover, all the samples, including those of the outlier SC-Unit, are aligned parallel to the trend of this compositional field, implying a roughly constant Zr/Nb ratio (which rules the inclination of the sub-rectilinear compositional fields), and accounting for a common origin from the MSVD.

A detailed petrographic description of the tephra layers that constitute the seven eruptive units of the MSVD Paleo-activity and the means of their correlation is provided as online supplementary material (Suppl. Mat. #1).

4.2.2 Morlupo activity (589±4 - 514±3 ka)

Based on geochronologic and stratigraphic data, we infer that the Morlupo center activity (de Rita et al., 1993) developed during three main stages: early (~0.59 Ma), middle (~0.55 Ma) and late (~0.51 Ma) activity phases.

4.2.2.1 Early phase: The Tufo Giallo di Castelnuovo di Porto eruptive cycle (589±4 ka)

The stratigraphic relationships of the products of this eruptive cycle, along with the position of the samples providing the chemo- and chrono-stratigraphic data presented in this paper are shown in Figure 5a.

Morlupo trachyte

Locally, a haüyne-bearing phono-trachytic scoria deposit (Morlupo trachyte, Cioni et al., 1993) crops out in the eastern sector of the MSVD, reaching a maximum thickness of 12 m near the town of Morlupo, where it lies on a thermometamorphosed Pliocene clay sedimentary succession. Based on this feature and on the $^{40}Ar/^{39}Ar$ age of 587±3 ka (Barberi et al., 1994), it has been previously interpreted to be the first eruptive product in the whole MSVD activity. The deposit shows the typical features of a near vent spatter-flow deposit, characterized by the presence of centimeter-sized, poorly vesicular scoria clasts within a dark grey ash matrix. The bulk XRF analysis of one sample (MOR 01, Figure 5 and 6, Appendix 5) confirms the trachytic composition of one sample analyzed in Conticelli et al. (1997).

In contrast, a 5 cm thick whitish pumice layer occurring at the base of the deposit (inset *a* in Figure 5) yielded the most alkaline phonolitic composition among all the MSVD products (MG-8, Figure 5 and 6, Table 4). Major element composition and mineral assemblage of pumice, with sanidine and

idiosyncratic accessory amphibole, coupled to the indistinguishable radiometric age, strongly suggests correlation of this layer to the Tufo Giallo di Castelnuovo di Porto.

Tufo Giallo di Castelnuovo di Porto (TGCP)

The Tufo Giallo di Castelnuovo di Porto (TGCP) is the largest pyroclastic-flow forming eruption of the Morlupo early phase of activity. It broadly matches the hydromagmatic ashy-pomiceous layers previously grouped into the 'Pyroclastic fall products from Morlupo edifice' unit, cropping out in the Morlupo area (de Rita et al., 1993). It is known in the litterature as 'Tufo di Riano' (Mattias and Ventriglia, 1970) or 'Tufo di Castelnuovo' p.p., which Mattias and Ventriglia (1970) describe to overlie the Morlupo trachyte (see below) and, in other localities, the Tufo Giallo della Via Tiberina. Pumice samples collected in the pyroclastic-flow deposit at Capena (Figure 1, 5) yielded a weighted mean age of 589±4 ka (Table 2). The depositional features from two localities (Castelnuovo di Porto and Morlupo; Figure 1, 5), including a ~1 m thick pumice fallout layer (here defined FAD-1) intercalated in the upper portion of the pyroclastic-flow deposit with no evidence of temporal break, are resumed in Figure 5a. Highly vesicular grey and white pumice in the TGCP pyroclastic-flow deposit is characterized by a mineral assemblage dominated by sanidine and including amphibole, which is quite uncommon in the MSVD products we have analyzed. Due to the pervasive crystallization of leucite (lct>30wt%), matrix glass in pumice, as well as in FAD 1, plots in the latite field (Figure 6a); however, a phonolitic composition for the original magma, similar to that of the MG8 sample, is inferable (Masotta et al., 2010).

Geochronologic and stratigraphic data (Figure 7, Table 3) allow us to correlate with the TGCP eruption several mid-distal pumice fall occurrences, matching in part the First Ashfall Deposits (FAD) of Karner et al. (2001), including Cave (591±3 ka; Marra et al., 2009), the INGV borehole (ING-02, 586±3 ka; Karner et al., 2001), and Fosso di Malafede (FoMF-C1, 595±6 ka; Marra et al., 2009) (Figure 1 and 7). The extensive occurrence of a pumice horizon at the base of the volcanic succession in Rome and as far as the eastern sector of the Colli Albani district (Marra et al., 2009),

testifies the Plinian character of the eruption responsible for its emplacement. The occurrence of an accretionary lapilli-rich ash deposit, that may be regarded as the distal equivalent of the TGCP pyroclastic-flow deposit, above a 5 cm-thick white pumice fall layer at both the mid- distal sections of GRA/A1 and Trigoria (Karner et al., 2001; Figure 1 and 7), suggests that these pumice fall occurrences may represent the early products of the TGCP eruption (FAD-0, Figure 7). However, their relationship with the main TGCP pyroclastic-flow deposit and with FAD-1 is uncertain.

Overall, the strict age concordance of the TGCP pyroclastic-flow deposit with the ~~the~~ distal pumice fall deposits and the Morlupo trachyte, combined to the near-vent facies of the latter, support the identification of the Morlupo center as the vent area of this phase of activity.

Trace-element compositional features of the TGCP eruptive cycle

The pyroclastic-flow deposit and one FAD 1 pumice sample define, along with one sample of the Morlupo trachyte (BR53, Conticelli et al., 1997), a very clustered and sub-rectilinear Zr/Y vs. Nb/Y compositional field (Figure 6b). In contrast, the pumice at the base of the Morlupo spatter-flow deposit displays very high Zr/Y and Nb/Y (sample MG-8, Figure 6b), a feature which characterizes all the pumices erupted in the early stages of each major eruptive cycle (e.g., samples of FAD-2, FAD-3A and PT2b-S2), and which is suggestive of a high degree of differentiation (Marra et al., 2011).

The three dated distal fallout samples, for which reliable major element analyses are not available, define a distinct, narrowly sub-rectilinear Zr/Y vs. Nb/Y field; a bulk sample of the pisolitic ash associated to the distal fallout deposits also yield similar Zr/Y vs. Nb/Y composition (TRIG, Figure 7 and 6b). The out-of-trend plotting of sample MOR 01 may reflect an intermediate composition between that of the main TGCP pyroclastic flow and that of the early fallout deposits (FAD 0).

4.2.2.2 Later Fallout Deposits: FAD-2 Eruption unit (558±14 ka)

Figure 5a shows the correlations among the fallout deposits emplaced in the time span 589-546 ka, partially revising those proposed in Karner et al. (2001). In particular, we recognized two different, geochronologically distinct, fallout deposits emplaced above FAD-1, here named FAD-2 (558±14 ka) and FAD-3 (546±5 ka). The different mean weighted age, although overlapping at two sigma errors, coupled to the different Zr/Y vs Nb/Y composition of the fallout deposit sampled at Ponte Galeria (Fall PG,) with respect to that sampled at Morlupo and Capena (FAD 3, FAD 3CM, FAD 3-CP) (Figure 6a, b) suggest indeed the occurrence of two distinct eruptive units. Moreover, the age of 546±5 ka yielded by FAD 3A at Capena, where it underlies the LTGVT (Figure 5), demonstrated the stratigraphic inconsistency for the age of 565±3 ka previously attributed to the LTGVT by Karner et al. (2001), and showed that emplacement of the FADs spanned a wider temporal range, with respect to the previously assumed age of 586±3 ka.

In an attempt to investigate the causes of the stratigraphic inconsistency of the previously published ages, we have re-evaluated the original data for sample R93-25A of LTGVT (Karner and Renne, 1998; GSA Data Repository item 9845) and have noted that it contains two populations of crystals that, due to the large associated errors, were not distinguished with a 2σ cutoff principle of exclusion (Karner et al., 1998) (see Appendix 3). Two youngest crystals yield ages of 548±24 and 549±24 ka, respectively, whereas the other four have errors spanning 4 to 12 ky, and yield a well-constrained weighted mean age of 565±3 ka. Based on the stratigraphic evidence at the Capena section of an age $\leq$546±5 ka for the LTGVT, we interpret the older population in sample R92-25A as a xenocrystic contamination, whereas we assume the weighted mean age of the two youngest crystals, here assessed at 549±16 ka, as that attributable to the LTGVT (R93-25A-1, Table 3). This age is undistinguishable from that of 546±5 ka obtained for the underlying FAD-3A, thus eliminating the stratigraphic inconsistency, and it is also consistent with that of 546±3 ka provided for the overlying Upper Tufo Giallo della Via Tiberina in Karner and Renne (1998) (sample R93-02, Figure 5, Table 3).

Moreover, the older age yielded by FAD 2 at Ponte Galeria (558±14 ka) is very similar to that yielded by the reworked crystals within the LTGVT (sample R93-25A-2: 565±3 ka, Table 3), suggesting that these crystals may have derived from the magma of the previous eruptive cycle, supporting the inference of two different eruptions emplacing FAD-2 and FAD-3. In particular, we attribute to the earlier event, FAD-2, also the white pumice layer described by Karner et al. (2001) at the base of the km 13 of Via Tiberina section (sample FAD 13, Figure 5), which displays identical TAS composition and similar Zr/Y vs Nb/Y signature to that of Fall PG (Figure 6a and 6b). Also, we suggest that the age value of 565±3 ka obtained on the xenocrystals within the LTGVT may constrain better the FAD-2 age with respect to the indistinguishable, but poorly constrained value of 558±14 ka, yielded by the pumice fall deposits sampled at Ponte Galeria. In contrast, according to the very different Zr/Y vs Zr/Y composition (Figure 6b) and the younger weighted mean age of 546±5 ka, we interpret FAD-3A as a distinct, later eruption unit opening the following TGVT eruption cycle.

4.2.2.3 Middle phase: The Tufo Giallo della Via Tiberina eruptive cycle (TGVT; 546±5 ka)

Based on intervening minor stratigraphic discontinuities and indistinguishable radiometric ages, we consider FAD-3, LTGVT and UTGVT as different eruption units of the same eruptive cycle that we name Tufo Giallo della Via Tiberina Eruptive Cycle (Figure 2, Table 1), and to which we assign the well constrained age of 546±5 ka obtained in this work on the earliest erupted product (FAD-3A, Table 2).

FAD-3 eruption unit

This unit includes a fallout deposit (FAD-3A) of well-sorted, cm-sized white pumice lapilli, with mm-sized accidental lithics of the Pliocene clay and the meso-Cenozoic carbonate substrates, which opens the major eruptive cycle leading to the emplacement of the Upper Tufo Giallo della Via

Tiberina (UTGVT) pyroclastic-flow deposit. The latter is one of the most voluminous eruptions in the whole MSVD activity, with a minimum erupted volume of 10 km^3 inferred from isopach maps of the residual outcropping portions (e.g. de Rita et al., 1993). The climactic phase is preceded by at least two eruptive episodes, separated by appreciable quiescence, as evidenced by two intervening, incipient paleosols between the early white pumice fall (FAD-3A), a second fallout deposit made up of grey, poorly vesicular scoria (FAD-3B), and the LTGVT (Figure 5).

The occurrence of FAD-3A only at the proximal Capena type-section and at several outcrops within the town of Morlupo indicates its provenance from this vent area. The indistinguishable eruption age, coupled to the pumice and lithic isopleth maps for the UTGVT pyroclastic-flow deposit (Figure 8a), provide evidence of a common vent area corresponding to the Morlupo center for the whole TGVT Eruption Cycle.

Lower Tufo Giallo della Via Tiberina eruption unit (LTGVT)

A 5-7-cm thick, laminated ashy surge layer (a in Figure 5b), followed by a 2-3 cm thick scoria lapilli fall layer (b in Figure 5b), represent the initial stages of the LTGVT eruption in the investigated, proximal sections. A faintly laminated, ash-flow deposit (c in Figure 5b), with abundant, cm-sized white pumice and accretionary lapilli, is present on top with a variable thickness, reaching up to several meters within paleovalleys. This flow-unit, based on a $^{40}Ar/^{39}Ar$ age of 561±1 ka on a sample collected in the Treja Valley near Calcata, was previously related to a distinct event with respect to the UTGVT (Karner et al., 2001). However, new data discussed in the previous sections evidence that no geochronologically appreciable time break occurred between the emplacement of FAD-3A and UTGVT, despite the occurrence of poorly developed soils above FAD3A and FAD-3B. Moreover, field observation for the present work lacks evidence of any significant discontinuity between the LTGVT and UTGVT pyroclastic-flow deposits, suggesting a co-eruptive origin.

Upper Tufo Giallo della Via Tiberina eruption unit a, b, c and d (UTGVT)

The UTGVT pyroclastic-flow deposit is characterized by a well-lithified, prevalent yellow ash matrix, containing abundant yellow pumice, accretionary lapilli, unmetamorphosed sedimentary lithic clasts, leucite and sanidine crystals, and subordinate lava clasts and clinopyroxene and biotite crystals.

Three main horizons corresponding to as many eruptive phases without any significant evidence of temporal break, consistent with the lack of intervening paleosols, are recognizable in the field (Karner et al., 2001). They are represented by two pyroclastic-flow deposits (Unit a and b), followed by alternating ash-, scoria-, and pumice-fall deposits (Unit c; Figure 5). These three units yielded indistinguishable $^{40}Ar/^{39}Ar$ ages, providing a weighted mean of 552±10 ka (Karner et al., 2001, Table 3), consistent with that of 546±3 ka yielded by the lower pyroclastic-flow unit sampled in the Riano quarries of Via Tiberina (Karner and Renne, 1998, Figure 5, Table 3).

A fourth unit (d) has been recognized in this work and interpreted as the deposit of the UTGVT late eruptive phase, based on its stratigraphic position above the main pyroclastic-flow deposit at the locality of Via Casale Francalancia (Figure 1), 4 km south of Morlupo, without any evidence of temporal break, and based on the occurrence of large ballistics (up to 20 cm in diameter), indicating its proximal facies.

Compositional features of the TGVT eruptive cycle

The compositional features of the TGVT Eruption Cycle have been discussed in detail by Masotta et al. (2010), who reported similar bulk trachy-phonolitic compositions for both white pumices and black grey scoria. The Zr/Y vs Nb/Y diagram allows to recognize a clustering of the different units of the TGVT eruption cycle in distinct compositional fields (Figure 6b). Some of these compositional fields, when represented by three samples at least, have also sub-rectilinear trends (e.g.: LTVT, FAD-3A), as previously outlined for the samples of TGCP and FAD-0 (Figure 6b).

However, apart from the least alkaline, dark scoria bulk samples plotting closer to the origin of the axes, the reasons why the white pumice samples of each different eruptive unit plot in different portions of the Zr/Y vs Nb/Y diagram are not easily reconciled with their homogeneous phono-trachytic bulk compositions. In any case, these Zr/Y vs Nb/Y signatures should be regarded as a distinctive feature of each erupted product, and used as a complementary tool for their correlation with distal equivalents.

4.2.2.4 Late phase: Prima Porta Eruptive Cycle (514±3 ka)

Tufo Giallo di Prima Porta (TGPP; 517±6 ka)

The Tufo Giallo di Prima Porta (TGPP) was distinguished by Karner et al. (2001) from the Tufo Giallo della Via Tiberina (to which it was previously attributed, de Rita et al., 1993), based on its stratigraphic position (above the Tufo del Palatino from Colli Albani, dated 530±2 ka, Karner et al., 2001) and $^{40}Ar/^{39}Ar$ age of 517±6 ka. It is a massive pyroclastic-flow deposit emplaced mainly in the southern MSVD sector within the Paleo-Tiber valley. In the outcrops of Prima Porta (Figure 1), it displays a well-lithified facies (Jackson et al., 2005), very similar to that of the units a and b of the UTGVT, except for a lower pumice clast content. It also contains scarce, although characteristic, grey, poorly vesicular, leucite- and clinopyroxene-bearing scoria clasts, up to 10 cm in diameter, and displays a distinctive grey-greenish color within the semi-lithified facies exposed along the southern tract of the Tiber valley, down to Rome (outcrops of the Capitol and Palatine Hills, Corazza et al., 2004).

An accretionary lapilli-rich ash layer, representing the co-ignimbrite ash-cloud deposit, occurs at the top of the pyroclastic flow deposit in several mid-distal sections. At the base of the pyroclastic flow deposit, a Plinian-style fallout deposit, made up of inversely graded, highly vesicular white pumice, lies on top of a mature, dark brown paleosoil and reaches a maximum thickness of 2.5 m in

the northern MSVD area. In Figure 8 b, representative pumice and lithic isopleths and isopachs define a SW–NE-trending dispersal axis and indicate the Morlupo center as the source area. The basal fallout pumice is characterized by vitrophyric texture (porphyricity index < 5% vol.) and high vesicularity (vol. < 50%; computed after Carey and Sparks, 1986; Fierstein and Nathenson, 1992). Rare euhedral sanidine (2 mm-sized) characterizes the phenocrysts assemblage, while sanidine and clinopyroxene are frequent in the groundmass.

Grottarossa Pyroclastic Sequence (513±3 ka)

A sequence of dark grey ashy pyroclastic flow and subordinate fall deposits, essentially constituted by mm- to cm-sized, poorly vesicular, dark grey scoria clasts with leucite, sanidine and clinopyroxene, occurs along the northern Tiber River Valley above the TGPP. Karner et al. (2001) identified four subunits in the Grottarossa Pyroclastic Sequence (GRPS –a through –d), including a characteristic stratigraphic marker represented by a zoned, orange to black scoria-fall layer (subunit b'-b"). The presence of small fossil trees at the base of each of the first three subunits suggests the occurrence of intervening dormancies. However, based on the ages for units a and b of 519±6 ka and 511±9 ka, respectively (samples PAL-01 and SAX-01, Table 3, Appendix 2), it is not possible to quantify the corresponding temporal gaps. We assessed the eruption age for the GRPS by the combined weighted mean age of these samples, plus one sample collected at Cava Rinaldi (CR1, 510±4 ka, Table 3 and 8) and attributed in this work to this eruption sequence (see below), obtaining 513±3 ka. Since this age is not statistically distinguished with respect to that of 517±6 yielded by TGPP, we consider all these deposits as part of a common eruptive cycle (Prima Porta Eruptive Cycle), with a combined weighted mean age of 514±3 ka (Table 6).

On top of GRPS subunit d, a faintly pedogenized ash layer is present in the type-section of Via di Grottarossa (Karner et al., 2001), overlain by a widespread lithic-rich breccia deposits, up to ~1 m thick, containing dominantly holocrystalline lithic clasts with mm-sized clinopyroxene and dark

mica, and subordinate lava lithic clasts. Juvenile scoria clasts, up to cm-sized, are poorly vesicular and porphyritic with mm-sized crystals of leucite. Although previously interpreted as the initial deposit of the following eruptive cycle (Tufi Terrosi con Pomici Bianche; Karner et al., 2001), dispersal area (Figure 8c) and depositional features (e.g., the occurrence of ballistic sags) suggest the Morlupo center as source area.

Compositional features of the Prima Porta Eruptive Cycle

One pumice sample of the basal fallout of the TGPP yields TAS composition and Zr/Y vs Nb/Y ratios comparable to those of the phonolitic white pumice of the UTGVT and FAD-2 (Figure 9a and b). In contrast, the composition of one bulk sample of the distinctive coarse greenish scoria (TGPP-ds) may be regarded as relatively primitive, consistent with its high MgO content (Appendix 5) and its lower position in the Zr/Y vs Nb/Y diagram (Figure 9b).

Samples of juvenile clasts in the lithic-rich breccia of the GRPS, including one EMP analysis on melt inclusion in clinopyroxene and two bulk XRF analyses on samples with LOI<3.5% (A and B in Figure 9), also display relatively primitive, phonotephritic compositions (Figure 9a).

4.2.3 Sella di Corno Fall Layer (523±10 ka, Gaeta et al., 2003)

A deeply altered pumice fall deposit, that we tentatively correlate to the Sella di Corno (SdC) Plinian fall layer cropping out in the Apennine mountain range and dated 523±10 ka (Gaeta et al., 2003), is intercalated at several localities between the UTGVT and the TGPP; however its source area remains undetermined.

No reliable major element analysis is available for this extremely altered (LOI 33.18%; Appendix 5) sample. However, the Zr/Y vs Nb/Y composition of one bulk sample collected at the type-locality, quite similar to that of the earliest Southern Sabatini activity of Fall A1 (Figure 10b), evidences a MSVD provenance for the SdC pumice fall deposit. Based on the age of 523±10 ka and the consistent stratigraphic position below the TGPP (517±6 ka), this deposit may be regarded as an

early product of the Southern Sabatini phase of activity, overlapping the late period of the Morlupo activity.

4.2.4 Southern Sabatini center (499±3 - 389±4 ka)

4.2.4.1 Tufi Terrosi Eruptive Cycle (499±3 - 490±4 ka)

The stratigraphy and the compositional features of the Tufi Terrosi con Pomici Bianche (TTPB; Karner et al., 2001) has been described in detail by Sottili et al. (2004), who recognized four eruptive units (A, B, C, D), mainly constituted of fallout deposits. These eruptive units comprise alternating layers of white pumice and grey scoria clasts, grouped into several sub-units, separated by thick, partially reworked and deeply altered ash beds. The fourth unit (Fall D) was emplaced during the early phase of the 452±2 ka Tufo Rosso a Scorie Nere pyroclastic-flow forming eruption, and is therefore treated in the corresponding section. A comprehensive stratigraphic scheme of the complex TTPB succession cropping out at the type localities of Isola Farnese and Casale del Gallo (Sottili et al., 2004) is reported in Figure 11.

Fall A, Fall B, Fall C

The high degree of alteration that affects the fallout deposits of the TTPB, mainly as a consequence of the prolonged weathering that the deposits underwent during MIS 13 interglacial phase (see Marra et al., 2011 for an in-depth discussion), makes it difficult to obtain high quality geochronological and geochemical data on these products. Here, we discuss age determinations on three samples out of a succession of four primary and two partially reworked pyroclastic deposits (CR1, CR4, CR5, CR6, CR6B, CR7, Figure 11), interbedded within lacustrine sediments of the

Valle Giulia Formation (Karner and Marra, 1998), in comparison with two previous ages for the TTPB (sample R93-11M, Karner et al., 2001; sample 08-ISFARNESE-01, Marra et al., 2011).

The age obtained for the volcaniclastic deposit CR1 occurring at the base of the Cava Rinaldi succession (510±4 ka), coupled with its lithological and petrographic features and the stratigraphic position above the TGPP, provides strong evidence of its correlation with the GRPS, which is dated 511±9 ka at Grottarossa (sample SAX-01, Karner et al., 2001; Figure 11, Table 3, Appendix 2). This age does not overlap those of the overlying TTPB pumice samples at Cava Rinaldi (499±3, 496±9 ka), indicating the occurrence of two geochronologically distinct eruption cycles. In contrast, it appears more problematic the correlation of the overlying fallout deposits with the Fall A, B and C units and sub-units identified by Sottili et al. (2004) in the proximal settings, due to the lack of analyzable glasses and to the large error associated with the $^{40}Ar/^{39}Ar$ age of Fall B at Isola Farnese (494±14 ka). Therefore, to overcome these difficulties, we will rely on trace element compositions, following the approach of Marra et al. (2011). These authors recognized distinct Zr/Y vs Nb/Y compositional fields pertaining to samples of Fall A1, Fall B1 and Fall C1 analyzed by Sottili et al. (2004) and Lancaster et al. (2010), and attributed two samples (GR, VT, Figure 10b) collected in the mid-distal sections of Grottarossa and km 12.6 of Via Tiburtina (Figure 1 and 11), to the lower Fall A1, based on their strict alignment with other four samples of this eruptive unit (CG-1, -2, -3, and IF, Figure 10b). Similarly, we correlate the two lowest pumice layers of Cava Rinaldi (samples CR4 and CR5) to the upper Fall A1 and to the Fall A2 subunits, respectively, based on their alignment in the Zr/Y vs Nb/Y diagram with samples CG5 and CG9 of these eruptive deposits analyzed in Sottili et al. (2004) (Figure 10b). This correlation is supported by the zoned character of the lowest fallout deposit of Cava Rinaldi, with alternating white pumice and grey scoria, a feature consistent with the proximal stratigraphy of upper Fall A1 and Fall A2 at Casale del Gallo (Sottili et al., 2004; Figure 11). In contrast, the petrographic features and the younger age (490±4 ka), which is statistically distinguished from that of CR5 (499±3 ka), strongly suggest correlation of sample R93-11M collected at Ponte Galeria with Fall B. Based on these correlations, we have assessed the

age of Fall A at 499±3 ka and that of Fall B at 490±4 ka, since these ages, due to the small associated errors, equate the combined mean weighted ages of the primary deposits attributed to these eruption units (CR5 plus CR6B, and 08-ISFARNESE-01 plus R93-11M, respectively).

No age determination is available for the subsequent Fall C deposit. Following the trace-element approach, indeed, we attribute also the upper grey scoria layers of Cava Rinaldi (samples CR6B, CR7) to Fall A2, excluding correlation with Fall C1. Despite a TAS composition similar to that of sample #1 of Fall C1 within or close to the MS-B field (dashed line in Figure 10a), samples CR6B and CR7 display tight Zr/Y vs Nb/Y compositions similar to those of Fall A and within the MS-A field of Figure 10b, corresponding to latitic bulk compositions. In contrast, samples of Fall C1 display a wide compositional range within the TAS and Zr/Y vs Nb/Y MS-B fields of Figure 10.

Compositional features of the TTPB eruptive cycle

The progressive clockwise rotation of the Zr/Y vs Nb/Y compositions from Fall B2 and Fall C1, to upper Fall A1/A2, and to lower Fall A1 in the diagram of Figure 10b is consistent with a phonotephritic-tephriphonolitic composition for the grey scoria and a more evolved, trachy-phonolitic one for the white pumice of these eruptive units. Similarly, the grey scoria clasts of subunit upper A2 plot closer to the origin of the axes with respect to the white pumice samples (Figure 10b), according to the other differentiation trend associated to the Zr/Y vs Nb/Y composition. These observations suggest the contribution of a progressively more primitive feeder magma in the final stages of each eruptive event of the TTPB Eruptive Cycle, i.e., Fall A2 upper (CR6b, CR7), Fall B2, and Fall C (sample #3). In particular, the progressive elongation of the Fall C1 samples in the Zr/Y vs Nb/Y diagram is likely to parallel a progressive contribution of a more primitive magma during eruption, passing from more (basal sample #1) to less evolved (upper sample #3) compositions.

4.2.4.2 Tufo Rosso a Scorie Nere Eruptive Cycle (452±2 ka)

Tufo Rosso a Scorie Nere (TRSN; 452±2 ka), Fall E (450±7 ka), Fall F (447±7 ka)

The TRSN Eruption Sequence comprises a basal Plinian fall deposit (Fall D, Sottili et al., 2004) and a voluminous ash and scoria flow deposit, characterized by the presence of coarse (up to 20 cm), highly vesicular black scoria. The strong vapor-phase crystallization of zeolite minerals occurring in the valley-fill portions confers a deep reddish color and strong lithification to the pyroclastic-flow deposit, hence the historical name of "Tufo Rosso a Score Nere" (Red Tuff with Black Scoria) (Mattias and Ventriglia, 1970). The unlithified facies are instead characterized by homogeneous dark grey color ("Tufo Grigio Sabatino", Mattias and Ventriglia, 1970). A certain degree of misplacement occurs in the literature about the identification of the TRSN erupted at 450 ka in the MSVD and the analogous pyroclastic-flow deposit with the same name erupted at 150 ka from the Vico volcano (Vico C; Cioni et al., 1993). Also the lithified facies of the TRSN characterized by the presence of elongated scoria or *fiamme*, commonly referred to as "Peperini listati", was previously misinterpreted as erupted by the Vico or the Vulsini districts, whereas the local names of "Piperno" and "Nenfro", which are commonly used for different pyroclastic products of these volcanoes, are sometimes attributed to the TRSN cropping out in the northern sector of the MSVD.

The TRSN pyroclastic flow was dated at 452±2 ka (Karner et al., 2001), in good agreement with the previous $^{40}Ar/^{39}Ar$ dating of 449±6 ka (Cioni et al., 1993). Based on the ages obtained in this work, it was rapidly followed by the emplacement of two Plinian-style pumice fall deposits, named Fall E and Fall F, at 450±7 and 447±7 ka, respectively (Figure 13, Table 2). Fall E reaches 50 cm in thickness at the Prima Porta type section with an eastward dispersal smaller than Fall A and B, which are spread southeast through the city of Rome and the Colli Albani area (Sottili et al., 2004; Marra et al., 2009). Fall F possibly shows an even more limited and eastward distribution: up to now it has been only recognized at the Prima Porta type section, in an outcrop located 4 km west of Morlupo, and at two sites along the eastern side of the Tiber River valley (Figures 1, 13).

Compositional features of the TRSN eruptive cycle

Glass compositions of the TRSN black scoria, the white pumice of basal Fall D and later Fall E plot at the transition between the trachyte and the phonolite fields; they define a strictly clustered compositional field (light grey area) in the TAS diagram (Figure 12a) together with the white pumices of Fall A and Fall B1 (short-dashed field). This is a distinct, higher-SiO_2 field with respect to that defined by the white pumice of the Morlupo eruption cycles (long-dashed field in Figure 12a). No analyzable glass occurs in the deeply altered Fall F deposit; however, EMP analyses of melt inclusions in clinopyroxene suggest a phono-tephritic magma composition.

In contrast to the clustered TAS compositions, the Zr/Y vs Nb/Y compositions of Fall D, TRSN and Fall E are spread through the MS-A field in Figure 12b, and overlap those of FAD-2, UTGVT and TGPP. The grey scoria of Fall F has instead a primitive MS-B composition in both diagrams of Figure 12.

4.2.4.3 Late Southern Sabatini Succession (389±4 - 379±40 ka)

No volumetrically significant eruptive activity occurred in the MSVD from 450 ka until around 315 ka, as suggested by the lack of corresponding products within this time span (Sottili et al., 2010), and also supported by the stratigraphy of the Via San Abbondio type-section (near the town of Riano; Figure 13), investigated in this work. At this locality, the late products of the Southern Sabatini activity overlie two pumice fall layers attributed to the early Vico activity (i.e., Vico α and Vico β of Cioni et al., 1987), based on stratigraphic and geochemical data presented in this paper (Figure 14b, Table 4, and Appendix 5).

In order to assess the provenance of the 412±2 ka and 418±6 ka "Bedded Pumice" of Karner et al. (2001), occurring within the fluvial-lacustrine deposits of the San Paolo Formation (Karner and Marra, 1998) at Ponte Galeria and at the Capitoline Hill (Rome), respectively (Figure 14a), we compared their geochemical composition to that of the coeval products from Vico (Vico α and Vico

β, 419±6 - 403±6 ka; Cioni et al., 1993; Barberi et al., 1994; = Rio Ferriera Formation, Perini et al., 2004), that we sampled at the type-locality of San Martino, 2 km south of Civita Castellana, and at Via San Abbondio (Figure 1, Figure 14b, c). The white pumice bulk samples from Ponte Galeria and Capitoline Hill (C7 and 07-FC-SP-01) display trachytic composition alike the bulk samples of the Rio Ferriera Formation analyzed by XRF technique (Perini et al., 2004; light grey field V1a in Figure 14b). The EMP glass compositions provided in the present work for the Vico-α samples, collected from the central portion of the deposits at San Martino and Via San Abbondio localities, representing the climactic eruption phase, plot at the rhyolitic extreme of this field. Consistent with the indistinguishable radiometric ages of the "Bedded Pumice" and Vico-α (the Vico-α deposit at San Martino yielded 412±7 and 419±6 ka; Barberi et al., 1994), their correlation can be thus assumed as reliable.

In addition, consistent with the compositional features of Period I of activity at Vico, ~~which is~~ characterized by a continuous mixing of latitic (V1b in Figure 14b) and trachytic magmas (V1a) (Cioni et al., 1987; Perini et al., 2004), we interpret the two dark scoria fall deposits dated at 427±5 and 412±5 ka (R94-30C and TDC-DSL) occurring at the sections of Prima Porta and Tenuta di Capannacce (Figure 1 and 13) to represent less differentiated products of the same phase of the Vico activity that emplaced the trachytic pumices. The identical Zr/Y vs Nb/Y signature of these dark scoria samples, plotting close to the Vico-α samples analyzed in this work (Figure 14c), strongly supports this correlation.

Based on these correlations, no products attributable to the MSVD are found between the TRSN Eruption Cycle and the San Abbondio Ash-lapilli Succession (SAAS), which is a rather homogeneous, more than 7 m thick deposit of alternating dark grey, poorly vesicular scoria lapilli and ash showing incipient pedogenization (Figure 13). Two samples collected at the base and at the top of the succession (SA- C5 and SA-C4) display MS-B magma composition on the Zr/Y vs Nb/Y diagram, and a consistent poorly differentiated TAS bulk composition (Figure 12). The SAAS may be related to a strombolian activity occurred after the end of the Southern Sabatini volcanic phase,

since 389±4 ka (Sample SA-C5; Table 2, Figure 13). A poorly constrained upper age of 379±40 ka has been obtained on a sample collected at the top of the SAAS (SA-C4, Figure 13).

5. Tephrostratigraphic implications

5.1 Compositional characterization of the MSVD eruptive products

Figure 15 summarizes the results of the geochemical and geochronological investigations performed in this work, aimed at characterizing the explosive activity occurred in the MSVD in the time span 800-370 ka. At least seven major eruptions emplacing five sub-Plinian to Plinian-style pumice fall horizons and two pyroclastic-flow deposits are recorded in the mid-distal setting during the earliest phase of activity spanning 808-614 ka (Figure 15a). Although no reliable major-element analyses are provided for these tephras, their Zr/Y vs Nb/Y signature indicates that they belong to the MSVD activity (Figure 15b). Nine, geochronologically distinct, major explosive cycles characterized the main MSVD activity between 589 and 447 ka, emplacing at least thirteen widespread fallout deposits, with an eastward to southeastward, far-reaching dispersal. A long, relative dormancy is recorded in the MSVD until ca. 315 ka, when a new volcanic phase started at the Bracciano center.

EMP glass compositions of the MSVD products are clustered in the trachy-phonolitic field of the TAS diagram (Figure 15d), except for a minority of products, erupted in the final stages of each large explosive cycle (Fall F, GRPS-e), which display more primitive, phonotephritic composition. This is in good agreement with previous studies on the effusive activity (Conticelli et al., 1987), showing a single series of evolution for the MSVD magma, from tephrites to phonolites.

Most of the analyzed products are characterized by Zr/Y vs Nb/Y compositions clearly distinguished from those of the other volcanic districts of Central Italy (Figure 15b-c), attesting that this geochemical signature can be used to identify the provenance from the MSVD of relatively altered deposits, in particular distal tephra layers, such as those of the MSVD Paleo-activity. In this

case, the good concordance of the Zr/Y vs Nb/Y compositions of two couples of tephra layers recovered in different boreholes and in different stratigraphic contexts (I9-B and PTS14-A, and I9-A and I7-A, Figure 16a), combined with their stratigraphic position (Figure 16b) allows us to identify them as derived from the same eruptions (Paleotiber Units B and C, respectively). This also allows us to compute a better-constrained mean weighted age for the eruptive events, by combining the ages of the samples (Figure 16a).

Although the very similar composition of sample PTS6-A and samples I7-A and I9-A would suggest their correlation (Figure 16a), geochronological and stratigraphic evidence instead suggests to assign the former one to a fourth, distinct unit (Unit d). This points out that the Zr/Y vs Nb/Y signature cannot be considered a unique feature of each eruptive unit. Therefore, other than stratigraphical, chronological or geochemical indicators, it represents an auxiliary tool to verify a possible correlation. Indeed, the following examples demonstrate that when used in combination with other geochemical indexes, e.g. by crossing trace-element and glass compositions, the trace-element dataset provided in this paper can be used to fingerprint the dated MSVD eruption units, allowing the identification of distal tephra layers.

5.2 Potential of the Zr/Y vs Nb/Y diagram for tephrostratigraphic purposes

We have shown above the potentiality of this method in attributing the mid-distal fallout deposits of Cava Rinaldi to Fall A2 sub-unit: in this case, the application has been used backward to assign the age of the dated mid-distal occurrences to the proximal, undated products. Obviously, the same procedure might be applied to tephra layers in distal settings and thus be used as a potential, additional tool for the broader purposes of tephrostratigraphy. In order to test the reliability of the Zr/Y vs Nb/Y for discriminating individual tephra layers, we applied this method to two distal fallout deposits occurring in the Middle Pleistocene sedimentary successions of central-southern Apennines, for which EMP glass compositions were available.

The first test was applied to the tephra layer SC3, from the Middle Pleistocene lacustrine sediments of the Mercure basin, southern Italy. Based on its EMP glass composition and Sr isotope ratio and on the $^{40}Ar/^{39}Ar$ ages of 516.5±3.6 ka and 493.1±10.9 ka of two sandwiching tephra layers, the SC3 layer has been confidentially attributed to the Plinian Fall A eruption (c 499 ka; Giaccio et al., 2014). The Zr/Y vs Nb/Y composition of the SC3 tephra (Figure 17a) confirms its attribution to the MSVD. In particular, SC3 plots closer to the lower Fall A1 pumice, supporting the correlation with the TTPB. On the other hand, in the Zr/Y vs Nb/Y diagram, the Fall A field overlaps that of the Sella di Corno fall deposit (Figure 17a), and thus it cannot be excluded a possible correlation of SC3 to the Sella di Corno unit. Indeed, only the combination of Zr/Y vs Nb/Y diagram with the ordinary major element glass composition allows us to unambiguously correlate the most differentiated composition (i.e., the phonolitic component) of the SC3 tephra to the basal white pumices of the zoned Fall A unit.

The second test has been applied to the SUL1/5-3 layer from the Middle Pleistocene lacustrine succession of the Sulmona basin, central Italy (see Giaccio et al., 2009, 2013a). The stratigraphic position of SUL1/5-3 between the Tufo di Bagni Albule tephra (ca. 530 ka; Giaccio et al., 2013a, b) and the Fall A (ca. 499 ka; SUL5-1c in Giaccio et al., submitted; Figure 15b) and Pozzolane Rosse (ca. 457 ka; Giaccio et al., 2013a) distal tephras, provides age constraints suggesting a possible correlation either with the TGPP (517±6 ka) or the Sella di Corno fallout (523±10 ka). Actually, EMP glass composition of SUL1/5-3 is compatible, yet not identical, to that of the TGPP, while a reference analysis for SdC is not available (Figure 17b). However, Zr/Y vs Nb/Y composition of sample SUL1-3 (Figure 17a), besides confirming the attribution to the MSVD activity, is quite similar to that of the SdC fallout, whereas it is incompatible with that of TGPP. Therefore, even in the lack of EMP data, the Zr/Y vs Nb/Y composition, coupled to the general chronostratigraphic context in which SUL1/5-3 occurs, allow us a confident attribution of this tephra to the SdC unit.

We remark that the slightly shifted position of the Zr/Y vs Nb/Y compositions of samples SC3 and SUL 1/5-3 with respect to those of the Fall A and Sella di Corno proximal samples in Figure 15a may reflect a small variation of the ratios, due to the different degree of porfiricity of the distal deposits with respect to the proximal ones.

Although the examples provided point out some limits of the Zr/Y vs Nb/Y diagram for tephrostratigraphic purposes, when applied in combination with the EMP glass composition, it may provide a fundamental tool, especially for the developing of the currently barely explored Middle Pleistoce tephrostratigraphy. It is known, in fact, that with exception of the very idiosyncratic Colli Albani volcanic tephras (Giacco et al., 2013b), the products from the intense, broadly contemporaneous, Middle Pleistocene explosive activities of the different ultrapotassic Peri-Tyrrhenian volcanoes (i.e., Vulsini, Sabatini, Vico and Roccamonfina) are compositionally rather monotonous and hardly discriminating each other via EMP composition, being dominated by similar trachy-phonolite/tephri-phonolite compositions (e.g., Peccerillo, 2005). For instance, it has been recently demonstrated that the EMP data alone are not sufficient for discerning the potential sources of a number of trachy-phonolite/tephri-phonolitic tephras of the Middle Pleistocene Mercure lacustrine succession (Giaccio et al., submitted), and this indeed applies to other Middle Pleistocene Italian tephrostratigraphic records (e.g., Acerno basin, Petrosino et al., in press). Only the combination of the EMP and Sr isotope data allowed the source of those Mercure tephra to be identified (Giaccio et al., 2014). In this perspective, the Zr, Y an Nb trace elements might indeed have a great potential, because their concentration in the pyroclastic deposits varies appreciably and significantly from district to district, much more than major elements (Marra and D'Ambrosio, 2012). In other words, similarly to what has been shown for the Sr isotopes (Giaccio et al., submitted), the Zr/Y vs Nb/Y diagram might be suitably used for discriminating the sources of tephras that display major element compositions compatible with different volcanoes and thus are not distinguishable on the basis of the EMP data alone.

Summary and concluding remarks

New stratigraphic and $^{40}Ar/^{39}Ar$ chronological data, major element electron microprobe (EMP) glass compositions, major and trace element XRF bulk compositions, and major and trace element FUS-ICP-MS bulk compositions have been obtained for the major eruptive units from the early phase of explosive activity (800-390 ka) in the Monti Sabatini Volcanic District (MSVD).

We have described and chronologically and compositionally characterized seven eruptive units: the Tufo Giallo di Castelnuovo di Porto (TGCP, 589±4 ka); the First Ash Fall Deposit 2 (FAD 2, 558±14 ka); the First Ash Fall Deposit 3 (FAD 3, 546±5 ka); the Fall A (499±3 ka – 496±9 ka) from the "Tufi Terrosi con Pomici Bianche" succession; the Fall E (450±6 ka) and Fall F (447±7 ka) from the "Tufi Stratificati Varicolori de La Storta"; and the San Abbondio Ash-lapilli Succession (SAAS, 389±4 ka). Moreover, compositional features have been obtained from previously dated MSVD units (Tufo Giallo di Prima Porta, Grotta Rossa Pyroclastic Sequence, Fall B and Fall C) and interbedded Plinian fall deposits from Vico volcanic district (Vico α and Vico β).

This new dataset substantially improve the general knowledge on the 0.8-0.4 Ma explosive activity of the Sabatini volcanic district and provides crucial and reliable data for tracing the individual investigated unit in distal settings, with significant implications for the development of Middle Pleistocene tephrostratigraphic studies in the Central Mediterranean area, hitherto prevented by the lack of robust reference data.

Under this perspective, in addition to provide the commonly used data for tephrostratigraphic purposes (e.g. EMP glass compositions and $^{40}Ar/^{39}Ar$ chronological data), here we have shown the potential of the trace elements for discriminating the volcanic sources of tephras sharing similar major element compositions.

Acknowledgements

$^{40}Ar/^{39}Ar$ age analyses performed for this work were funded by Istituto Nazionale di Geofisica e Vulcanologia, Italy. FUS-ICP-MS analyses were co-funded by INGV, Dipartimento di Scienze della Terra, Sapienza-Università di Roma, Italy, and Department of Geosciences - Georgia State University - Atlanta, U.S.A. We wish to thank Danilo Chiocchini of the Dipartimento di Scienze della Terra of the University of Perugia, who performed XRF chemical analyses, and Marcello Serracino of CNR-IGAG of Rome, for technical assistance during the EMP analyses.

Finally, we acknowledge Gianni Zanchetta for insightful suggestions on a previous version of this manuscript and Gianluca Iezzi for his detailed review; both contributions helped us to improve the quality of this work.

Supplementary material provided online

Supplementary Material item #1: Petrographic features of the volcanic products of the MSVD Paleo-activity

Appendix 1 - Full $^{40}Ar/^{39}Ar$ data performed at the University of Wisconsin-Madison Rare Gas Geochronology Laboratory.

Appendix 2 - Full $^{40}Ar/^{39}Ar$ data performed at the Berkeley Geochronology Center on the Cava Rinaldi samples.

Appendix 3 - Weighted mean ages re-calculated in this work from original reduction data in Karner and Renne, 1998 and Karner et al., 2001a.

Appendix 4 - Full EMP analytical compositions of samples analyzed in this work.

Appendix 5 - Major and trace element compositions of samples analyzed by Fusion ICP-MS at Activation Laboratories, Ancaster, Ontario, Canada.

References

Alvarez, W., 1972. The Treia valley north of Rome: volcanic stratigraphy, topographic evolution, and geological influences on human settlement. Geologica Romana 11, 153-176.

Alvarez, W., 1973. Ancient course of the Tiber river near Rome: an introduction to the Middle Pleistocene volcanic stratigraphy of Central Italy. Geol. Soc. Am. Bull. 84, 749-758.

Alvarez, W., Gordon, A., Rashak, E. P., 1975. Eruptive Source of the "Tufo Rosso a scorie Nere", a Pleistocene Ignimbrite North of Rome. Geologica Romana 14, 141-145.

Barberi, F., Buonasorte, G., Cioni, R., Fiordelisi, A., Foresi, L., Iaccarino, S., Laurenzi, M.A., Sbrana, A., Vernia, L., Villa, I.M., 1994. Plio-Pleistocene geological evolution of the geothermal area of Tuscany and Latium. Mem. Descr. Carta Geol. d'It. 49, 77-134.

Cann, J.R., 1970. Rb, Sr, Y, Zr, Nb in some ocean floor basaltic rocks. Earth Planet. Sci. Lett. 10, 7-11.

Carey, S.N., Sparks, R.S.J., 1986. Quantitative models of the fallout and dispersal of tephra from volcanic eruption columns. Bull. Volcanol. 48, 109-125.

Cioni, R., Sbrana A., Bertagnini, A., Buonasorte, G., Landi, P., Rossi, U., Salvati, L., 1987. Tephrostratigraphic correlations in the Vulsini, Vico and Sabatini volcanic successions. Periodico di Mineralogia 56, 137-155.

Cioni, R., Laurenzi, M.A., Sbrana A., Villa I.M., 1993. $^{40}Ar/^{39}Ar$ chronostratigraphy of the initial activity in the Sabatini volcanic complex (Italy). Boll. Soc. Geol. It. 112, 251-263.

Conticelli, S., Francalanci, L., Manetti, P., Cioni, R., Sbrana, A., 1997. Petrology and geochemistry of the ultrapotassic rocks from the Sabatini Volcanic District, central Italy: the role of evolutionary processes on the genesis of variably enriched alkaline magmas. J. Volcanol. Geotherm. Res. 75, 107-136.

Corazza, A., Lombardi, L., Marra, F., 2004, La geologia del Colle Capitolino. Il Quaternario 17, 413-441.

Corda L., de Rita D., Tecce F., Sposato A., 1978. Le piroclastiti del sistema vulcanico sabatino: il complesso dei tufi stratificati varicolori de La Storta. Boll. Soc. Geol. Ital. 27, 353-366.

de Rita, D., Funiciello, R., Rossi, U., Sposato, A., 1983. Structure and evolution of the Sacrofano-Baccano caldera, Sabatini Volcanic Complex, Rome: J. Volcanol. Geotherm. Res. 17, 219-236.

de Rita, D., Funiciello, R., Corda, L., Sposato, A., Rossi, U., 1993. Volcanic Units. In: Di Filippo, M., (Ed.), Sabatini Volcanic Complex, Quad. Ric. Sci. 114, Progetto Finalizzato Geodinamica C.N.R., Roma, 33-79.

Fierstein, J., Nathenson, M., 1992. Another look at the calculation of fallout tephra volumes. Bull. Volcanol. 54, 156-167.

Florindo, F., Karner, D.B., Marra, F., Renne, P.R., Roberts A.P., Weaver, R., 2007. Radioisotopic age constraints for glacial terminations IX and VII from aggradational sections of the Tiber River delta in Rome, Italy. Earth Planet. Sci. Lett. 256, 61-80.

Floyd, P.A., Winchester, J.A., 1975, Magma type and tectonic setting discrimination using immobile elements. Earth Planet. Sci. Lett. 27, 211-218.

Franzini, M., Leoni M., Saitta, M., 1972. A simple method to evaluate the matrix effects in X-ray fluorescence analysis. Spectrometry 1, 151-154.

Foley, S., Jenner, G., 2004. Trace element partitioning in lamproitic magmas - the Gaussberg olivine leucitite. Lithos 75, 19-38. doi: 10.1016/j.lithos.2003.12.020.

Gaeta, M., Palladino, D.M., Karner, D.B., Renne, P.R., 2003. Vulcanoclastiti della Valle del Corno (vvc). In: Centamore E., Dramis F., (Eds.), Note Illustrative della Carta Geologica d'Italia alla scala 1:50.000 - foglio 358 Pescorocchiano. Regione Lazio, 34-35.

Galli, P., Giaccio, B., Messina, P., 2010. The 2009 central Italy earthquake seen through 0.5 Myr-long tectonic history of the L'Aquila faults system. Quaternary Science Reviews 29, 3768e3789.

Giaccio B, Messina P, Sposato A, et al. 2009. Tephra layers from Holocene lake sediments of the Sulmona basin, central Italy: implications for volcanic activity in peninsular Italy and tephrostratigraphy in the central Mediterranean area. Quaternary Science Reviews 28: 2710–2733.

Giaccio, B., Arienzo, I., Sottili, G., Castorina, F., Gaeta, M., Nomade, S., Galli, P., Messina P., 2013a. Isotopic (Sr-Nd) and major element fingerprinting of distal tephras: an application to the

Middle-Late Pleistocene markers from the Colli Albani volcano, central Italy. Quaternary Science Reviews 67, 190-206.

Giaccio, B., Castorina, F., Nomade, S., Scardia, G., Voltaggio, M., Sagnotti, L., 2013b. Revised chronology of the Sulmona lacustrine succession, central Italy. Journal of Quaternary Science, in print. DOI: 10.1002/jqs.2647.

Giaccio, B., Galli, P., Peronace E., Arienzo, I., Nomade, S., Cavinato, G.P., Mancini, M., Messina, P., Sottili, G., 2014. A 560-440 ka tephra record from the Mercure basin, southern Italy: volcanological and tephrochronological implications. Journal of Quaternary Sciences, in print.

Jackson, M.D., Marra, F., Hay, R.L., Cawood, C., Winkler, E., 2005. The judicious selection and preservation of tuff and travertine building stone in ancient Rome. Archaeometry 47, 3, 485–510.

Karner, D.B., Renne, P.R., 1998. $^{40}Ar/^{39}Ar$ geochronology of Roman Volcanic Province tephra in the Tiber River Valley: Age calibration of middle Pleistocene sea-level changes. Geol. Soc. Am. Bull. 110, 740-747.

Karner D.B. & Marra F., 1998. Correlation of Fluviodeltaic Aggradational Sections with Glacial Climate History: A Revision of the Classical Pleistocene Stratigraphy of Rome. Geol. Soc. Am. Bull. 110, 748-758.

Karner, D.B., Juvigne´, E., Brancaccio, L., Cinque, A., Russo Ermolli, E., Santangelo, N., Bernasconi, S., Lirer, L., 1999. A potential early middle Pleistocene tephrostratotype for the Mediterranean Basin: the Vallo di Diano, Campania, Italy. Global and Planetary Change 21, 1–15.

Karner, D.B., Marra, F., Renne, P., 2001. The history of the Monti Sabatini and Alban Hills volcanoes: groundwork for assessing volcanic-tectonic hazards for Rome. J. Volcanol. Geotherm. Res. 107, 185-219.

Kaye, M.J., 1965. X-ray fluorescence determinations of several trace elements in some standard geochemical samples. Geochemistry and Cosmochemistry Acta 29, 139-142.

Kuiper, K.F., Deino, A., Hilgen, F.J., Krijgsman, W., Renne, P.F., Wijbrans, J. R., 2008. Synchronizing rock clocks of Earth history. Science 320, 500–504. doi:10.1126/ science.1154339.

Lancaster, L.C., Sottili, G., Marra, F., Ventura G., 2010. Provenancing of Light Weight Volcanic Stones Used in Ancient Roman Concrete Vaulting: Evidence from Rome. Archaeometry 53, 707-727. doi: 10.1111/j.1475-4754.2010.00565.x

Laurenzi, M.A., Villa, I.M., 1987. $^{40}Ar/^{39}Ar$ chronostrastigraphy of Vico ignimbrites. Periodico di Mineralogia 56, 285-293.

Lowe, D.J., 2011. Tephrochronology and its application: A review. Quaternary Geochronology 6, 107-153.

Marra, F., Florindo, F., Karner, D.B., 1998. Paleomagnetism and geochronology of early Middle Pleistocene depositional sequences near Rome: comparison with the deep sea δ^{1}□O climate record. Earth Planet. Sci. Lett. 159, 147-164.

Marra, F., Florindo, F., Boschi E., 2008. The history of glacial terminations from the Tiber River (Rome): insights to glacial forcing mechanisms. Paleoceanography 23, PA2205. doi:10.1029/2007PA001543.

Marra, F., Karner, D.B., Freda, C., Gaeta, M., Renne, P.R., 2009. Large mafic eruptions at the Alban Hills Volcanic District (Central Italy): chronostratigraphy, petrography and eruptive behavior. Journ. of Volc. and Geoth. Res. 179, 217-232. doi:10.1016/j.jvolgeores.2008.11.009

Marra, F., Deocampo, D., Jasckson, M.D., Ventura, G., 2011. The Alban Hills and Monti Sabatini volcanic products used in ancient Roman masonry (Italy): an integrated stratigraphic, archaeological, environmental and geochemical approach. Earth-Science Reviews 108, 115-136. doi:10.1016/j.earscirev.2011.06.005

Marra, F., D'Ambrosio, E., Sottili, G., Ventura G., 2012. Geochemical fingerprints of volcanic materials: Identification of a pumice trade route from Pompeii to Rome. Geol. Soc. Am. Bull., in print. doi: 10.1130/B30709.1

Marra, F., D'Ambrosio, E., 2012. Trace-element classification diagrams of pyroclastic rocks from the volcanic districts of Central Italy: the case study of the ancient Roman ships of Pisa. Archaeometry, in print. doi: 10.1111/j.1475-4754.2012.00725.x

Masotta, M., Gaeta, M., Gozzi, F., Marra, F., Palladino, D.M., Sottili, G., 2010. H_2O- and temperature-zoning in magma chambers: the example of the Tufo Giallo della Via Tiberina eruptions (Sabatini Volcanic District, central Italy). Lithos 118, 119-130.

Mattias, P.P., Ventriglia, U., 1970. La regione vulcanica dei monti Sabatini e Cimini. Mem. Soc. Geol. It. 95, 831-849.

Min, K., Mundil, R., Renne, P.R., Ludwig, K.R., 2000. A test for systematic errors in 40Ar/39Ar geochronology through comparison with U/Pb analysis of a 1.1-Ga rhyolite. Geochemical Cosmochemical Acta 64, 73-98.

Munno, R., Petrosino, P., Romano, P., Russo Ermolli, E., Juvigne´ , E., 2001. A late Middle Pleistocene climatic cycle in southern Italy inferred from pollen analysis and tefrostratigraphy of the Acerno lacustrine succession. Geographie physique et Quaternaire 55, 87–99.

Nappi G., De Casa, G., Volponi, E., 1979. Geologia e caratteristiche tecniche del 'Tufo Giallo della Via Tiberina'. Mem. Soc. Geol. It. 98, 431-445.

Pearce J.A., Cann J.R., 1973. Tectonic setting of basic volcanic rocks determined using trace element analyses. Earth. Planet. Sci. Lett. 19, 290-300.

Pearce J.A., Norry, M., 1979. Petrogenetic Implications of Ti, Zr, Y, and Nb Variations in Volcanic Rocks. Contrib. Mineral. Petrol. 69, 33-47.

Pearce, J.A., 1996. A users guide to basalt discrimination diagrams, Trace Element Geochemistry of Volcanic Rocks: Applications for Massive Sulphide Exploration. Geological Association of Canada, Short Course Notes 12, 79-113.

Peccerillo, A., 2005. Plio-Quaternary volcanism in Italy: Petrology, geochemistry, geodynamics. Springer-Verlag, Berlin.

Perini, G., Francalanci, L., Davidson, J.P., Conticelli, S., 2004, Evolution and genesis of magmas from Vico volcano, Central Italy: multiple differentiation pathways and variable parental magmas. Journal of Petrology 45, 139–182.

Petrosino, P., Jicha, B., Mazzeo, F.C., Russo Ermolli, E.A. High resolution tephrochronological record of MIS 14-12 in the Southern Apennines (Acerno basin, Italy). Jour. of Volcanol. and Geotherm. Res., in print.

Scherillo, A., 1940, I tufi litoidi a scorie nere della regione Sabazia e Cimina. Periodico di Mineralogia 11, 301-338.

Scherillo, A., 1947. I Vulcani Sabatini. Bollettino della Società Naturalista di Napoli 55, 125-130.

Smith, M.E., Singer, B.S., Carroll, A.R., Fournelle, J.H., 2008. Precise dating of biotite in distal volcanic ash: Isolating subtle alteration using $^{40}Ar/^{39}Ar$ laser incremental heating and electron microprobe techniques. American Mineralogy 93, 784-795.

Sottili, G., Palladino D.M., Zanon V., 2004. Plinian activity during the early eruptive history of the Sabatini Volcanic District, Central Italy. Jour. of Volcanol. and Geotherm. Res. 135, 361-379.

Sottili, G., Palladino, D.M., Marra, F., Jicha, B., Karner, D.B.,and Renne, P.F., 2010. Geochronology of the most recent activity in the Sabatini Volcanic District, Roman Province, central Italy. Jour. of Volcanol. and Geotherm. Res. 196, 20-30.

FIGURE CAPTIONS

Figure 1) Digital elevation map of the studied area showing location of: a) type-sections described in the present work; b) other investigated sites; c) boreholes; d) buried fault.

Figure 2) Composite chronostratigraphic log of the Monti Sabatini Volcanic District, showing the relationships with the mid-distal deposits intercalated within the fluvio-lacustrine successions of the Paleo-Tiber River. Location of the samples dated by $^{40}Ar/^{39}Ar$ method in this and previous work is also shown.

Figure 3) a) Zr/Y vs. Nb/Y compositional fields of the different volcanic districts of the Roman Magmatic Province compared to the distribution of all the samples of the Monti Sabatini Volcanic District for which trace-element analyses are provided in the literature (modified from Marra and D'Ambrosio, 2012). One principal compositional field for the MSVD (MS-A') displays very limited overlap with those of all the other districts, allowing for identification of the source area of the products. Compositional fields for the Colli Albani products from Marra et al. 2011: PR: Pozzolane Rosse; PN: Pozzolane Nere; VS: Villa Senni Eruptive Sequence; b) Zr/Y vs. Nb/Y compositions of the samples of the Paleo-activity of the MSVD. Location of the boreholes (PT2b, I9, I7, PTS6, PTS14, ING01), dated tephra occurrences and analyzed samples are shown in Figure 1.

Figure 4) a) Total alkali vs. silica (TAS) EMP glass compositions of 22 samples analyzed in this work (Table 4, Appendix 4); b) Average EMP glass compositions to compare with the Zr/Y vs. Nb/Y diagrams for all the bulk and glass samples (c).

Figure 5) a) Chrono-stratigraphic relationships of the products of the Tufo Giallo di Castelnuovo di Porto and Tufo Giallo della Via Tiberina eruptive cycles, from the type sections described in this

and in previous work (see Figure 1 for location). The location of the dated (Table 2, 3) and analyzed (Table 4, 5, Appendix 4, 5) samples is shown; b) Photographs of the volcanic deposits cropping out at the type-sections of Morlupo and Capena.

Figure 6) a) EMP glass and selected bulk compositions in the TAS diagram; b) Zr/Y vs. Nb/Y compositions of samples of the Tufo Giallo di Castelnuovo di Porto and Tufo Giallo della Via Tiberina eruptive cycles, analyzed in this work.

Figure 7) Chrono-stratigraphic relationships among the mid-distal exposures of the Tufo Giallo di Castelnuovo di Porto eruptive cycle described in previous literature (see Figure 1 for location), with respect to the proximal exposures described in this work. The location of the dated (Table 2, 3) and analyzed (Table 4, 5, Appendix 4, 5) samples is shown.

Figure 8) Isopach and pumice/lithic isopleth maps for different eruptive units of the Tufo Giallo della Via Tiberina, Tufo Giallo di Prima Porta, and Grottarossa Pyroclastic Sequence eruptive cycles, showing a common vent area corresponding to the Morlupo Center.

Figure 9) EMP glass and selected bulk compositions in the TAS diagram (a), compared to Zr/Y vs. Nb/Y compositions (b), of samples from the Tufo Giallo di Prima Porta and Grottarossa Pyroclastic Sequence eruptive cycles, analyzed in this work.

Figure 10) EMP glass and selected bulk compositions in the TAS diagram (a), compared to Zr/Y vs. Nb/Y compositions (b), of samples from the Tufi Terrosi con Pomici Bianche (TTPB) eruptive cycle, analyzed in this work.

Figure 11) Chrono-stratigraphic relationships of the products of the Tufi Terrosi con Pomici Bianche (TTPB) eruptive cycle, from type sections described in this and previous work (see Figure 1 for location). The position of the dated (Table 2, 3) and analyzed (Table 4, 5, Appendix 4, 5) samples is also shown.

Figure 12) EMP glass and selected bulk compositions in the TAS diagram (a), compared to Zr/Y vs. Nb/Y compositions (b), of samples from the Tufo Rosso a Scorie Nere eruptive cycle and of the following activity in the Southern Sabatini source area, analyzed in this work.

Figure 13) Chrono-stratigraphic relationships of the products of the Tufo Rosso a Scorie Nere eruptive cycle and of the following activity in the Southern Sabatini source area, from type sections described in this and previous work (see Figure 1 for location). The position of the dated (Table 2, 3) and analyzed (Table 4, 5, Appendix 4, 5) samples is shown.

Figure 14) a) Chrono-stratigraphic relationships of the products attributed to Period I of Vico activity, from type sections described in this and previous work (see Figure 1 for location). The position of the dated (Table 2, 3) and analyzed (Table 4, 5, Appendix 4, 5) samples is also shown; b) TAS bulk compositions of pyroclastic products of the two first activity periods of the Vico volcano (Perini et al., 2004; V1, V2: grey shaded areas), compared to the EMP glass and bulk compositions of nine samples attributed to Vico (this work); c) Zr/Y vs. Nb/Y compositions of seven samples of Vico products analyzed in this work

Figure 15) Synoptic overview of the chemo- and chronostratigraphic features of the MSVD. a) MSVD eruptive history in the time span 800 - 300 ka For individual eruptive events emplacing pumice and scoria fall deposits, the VEI is qualitatively assessed by comparison with eruptive parameters of Fall A1, B1, C and D reported in Sottili et al. (2004). Volumes of pyroclastic-flow

deposits are qualitatively assessed based on thickness and dispersal patterns. Bulk compositions of relatively unaltered samples (LOI <6.0%) are reported to integrate the Nb/Y vs Nb/Y signature, as a mean for identification of distal deposits. b) Zr/Y vs Nb/Y compositions of all the MSVD and Vico samples analyzed in this work compared to those from the other volcanic districts (after the critical review of Marra and D'Ambrosio, 2012). c) Zr/Y vs Nb/Y compositions of the major pumice fall deposits of MSVD and Vico. d) EMP glass compositions of the juvenile eruption products from the Morlupo and Southern Sabatini source areas.

Figure 16) Cross section showing the stratigraphy of the five boreholes in which the tephra layers of the Paleotiber eruptive succession were recovered (see location in Figure 1). See suppl. mat. #1 for criteria of correlation and assessment of the eruption ages.

Figure 17) Zr/Y vs Nb/Y (a) and TAS EMP glass (b, c) compositions of two distal tephra layers sampled in the lacustrine successions of the Mercure (SC3) and Sulmona (SUL1/5-3) basins, providing correlation with the MSVD products.

Table 1

THIS WORK				KARNER ET AL., 2001	DE RITA ET AL., 1993	MATTIAS & VENTRIGLIA 1970
VENT		ERUPTIVE CYCLE	ERUPTIVE UNIT			
	SOUTHERN SABATINI	Late Southern Sabatini Succession	Top *379±40* Sant'Abbondio Ash-lapilli Succession Bottom **389±4**		Pyrpoclastic fall products from Sacrofano and local scoria cones	Tufi Stratificati Varicolori di La Storta
VICO			CAP DSL **412±5**	Bedded Pumice *416±6*(1); *410±1*(1)		
			Vico α(4) **418±6; 412±2**			
			R94 -30C **427±5**			
		Tufo Rosso a Scorie Nere Eruptive Cycle **452±2**	Fall F **447±7**			
			Fall E **450±7**			
			Tufo Rosso a Scorie Nere **452±2**	Tufo Rosso a Scorie Nere 449±1(1)	Tufo Rosso a Scorie Nere sabatino	Piperno; Peperini listati
			Fall D			
		Tufi Terrosi Eruptive Cycle **499±3 ÷ 490±4**	Fall C (Sottili et al. (2004))	Tufi Terrosi con Pomici Bianche *488±2*(1)	Pyrpoclastic fall products from Sacrofano and local scoria cones	Tufi Stratificati Varicolori di Sacrofano
			Fall B **490±4** (Sottili et al. (2004))			
			Fall A **499±3** (Sottili et al. (2004))			
	MORLUPO	Prima Porta Eruptive Cycle **514±3**	Grottarossa Pyroclastic Sequence **513±3**	Grottarossa Pyroclastic Sequence *514±5*(1)		
			Tufo Giallo di Prima Porta **517±6**	Tufo Giallo di Prima Porta 514±3(1)	Sacrofano lower pyroclasatic flow unit	Tufo di Castelnuovo p.p.
		Tufo Giallo della Via Tiberina Eruptive Cycle **546±3**	Upper TGdVT **546±3**	Upper TGdVT *548±4*(1)		Tufo Giallo della Via Tiberina
			Lower TGdVT	Lower TGdVT *561±1*(1)	Morlupo p.f. unit	
			FAD 3 **546±5**	First Ash-fall Deposit (ING-02) *582±1*(1)	Pyroclastic fall products from Morlupo Edifice	Tufo di Riano Tufo di Castelnuovo p.p.
		FAD 2 **558±14** (565±3)(5)				
		Castelnuovo di Porto Eruptive Cycle **589±4**	FAD 1			
			Tufo Giallo di Castelnuovo di Porto **589±4** (Morlupo Spatter-flow)			Trachite di Morlupo
	PALEOMS	Santa Cecilia Eruption Unit **614±3**		614±3(2); *605±11*(2)		
		Vigna Murata Eruption Unit **653±4**		ING-01 Bis 649±4(1)		
		Ponte Galeria Eruption Unit **760±6**		Early airfall tuff, Ponte Galeria *758±4*(1)		
		Paleotiber Succession	Unit D **788±13** Unit C **801±9** Unit B **805±9** Unit A **808±6**	PT-S6 *783±7*(3) PT-2bS2 802±3(3)		

TABLE 1 - Summary chronostratigraphy of the MSVD provided in this work and correlation to previous nomenclature.
Ages performed for this work are calibrated to the Fish Canyon Tuff sanidine standard age of 28.201 Ma (Kuiper et al., 2008) and are reported with 2 σ uncertainty, those from previous works are at 1 σ and were calculated according to the following ages for the standard: (1) 27.84 Ma in Karner and Renne, 1998; (2) and (3) 28.02 Ma in Karner et al., 2001, and Florindo et al., 2007, respectively. In regular character are the ages of samples maintained to date the eruption cycles in this work after re-calculation. (4) Vico α defined by Cioni et al. (1987) was dated 419±6 ka (Laurenzi and Villa, 1987), and corresponds to the Rio Ferriera Formation of Perini et al. (2004).
(5) If assessed at the less conservative age estimation of 565±3 ka (see text for discussion) FAD 2 has to be considered a geochronologically distinct eruptive cycle.

Table 2

Table 2. Summary of $^{40}Ar/^{39}Ar$ data

Unit	Sample	Mineral	# of analyses	Weighted mean Age (ka)	± 2	MSWD	Reference
CAP DSL (Vico)	06-DEO-CAP-12*	biotite	10/10	398	± 19	0.23	Marra et al., 2011
VICO	07-FC-SP-01*	sanidine	10/10	418	± 6	1.15	Marra et al., 2011
Fall B	08-ISFARNES-01*	sanidine	10/10	494	± 14	0.21	Marra et al., 2011
SAAS bottom	C5 SA	sanidine	12/12	389	± 4	0.65	This Work
Fall F	Fall F-PP	sanidine	12/12	447	± 7	1.28	This Work
Fall E	Fall E-PP	sanidine	12/12	450	± 6	0.96	This Work
Fall A2	CR6-B	sanidine	14/14	496	± 9	0.97	This Work
FAD 3	FAD-3	sanidine	13/13	546	± 5	0.83	This Work
FAD 2	FALL-PG	sanidine	12/12	558	± 14	0.29	This Work
TGCP	TGCP-B	sanidine	15/15	589	± 4	1.20	This Work

Ages relative to 28.201 Ma for Fish Canyon sanidine (Kuiper et al. 2008) using Min et al. (2000) decay constant.

Full 40Ar/39Ar data in Appendix 1.

All analyses are single crystal fusions except for samples FAD-3 and TGCP-3, which were 3 and 4 crystal fusions, respectively.

Ages of samples marked * from Marra et al. (2011), originally calculated relative to the age of 28.02 Ma for Fish Canyon sanidine standard, have been re-calculated here according to the age of 28.201 Ma

LEGEND: SAAS: Sant'Abbondio Ash-lapilli Succession; TGCP: Tufo Giallo di Castelnuovo di Porto; FAD: First Ashfall Deposit.

Table 3

Table 3. Summary of 40Ar/39Ar data

UNIT	SAMPLE	LAB. NUMBER	MINERAL	No. OF ANALYSES	AGE (ka)	±2	MSWD	ORIGINAL REFERENCE	RECALCULATED AGE (ka	±2	
PT A	PT2b-S2	10813	sanidine	6/8	802.4	5.8	1.5	Florindo et al., 2007	**807.5**	**5.8**	rel to 28.201 Ma FC
PT B	I9-B	33180 + 33179	sanidine+leucite	14/15	^803,7	10.4	0.9	Florindo et al., 2007	**808.7**	**10.5**	rel to 1.201 Ma ACS
PT B	I9-BL	33179	leucite	7/7	^804.6	10.4	1.3	Florindo et al., 2007	**809.3**	**10.5**	rel to 1.201 Ma ACS
PT B	I9-BS	33180	sanidine	7/8	^793.6	15.8	0.1	Florindo et al., 2007	**798.3**	**15.9**	rel to 1.201 Ma ACS
PT B	PTS14-A	33178	sanidine	7/8	^795,2	10.8	1.5	Florindo et al., 2007	**800.2**	**10.8**	rel to 1.201 Ma ACS
PT C	I7-A	33181	sanidine	5/6	^799,3	12.4	0.2	Florindo et al., 2007	**804.3**	**12.5**	rel to 1.201 Ma ACS
PT C	I9-A	33182	sanidine	7/8	^783,7	13.4	0.2	Florindo et al., 2007	**788.6**	**13.5**	rel to 1.201 Ma ACS
PT C	PTS6-A	11083	sanidine	13/13	783.1	13.2	0.4	Florindo et al., 2007	**788.1**	**13.3**	rel to 28.201 Ma FC
PG	R93-12F	30189	sanidine	6/6	754	14		Karner and Renne, 1998	**758.8**	**14.1**	rel to 28.201 Ma FC
PG	R95-16A	7576	sanidine	3/15	758	8		Karner and Renne, 1998	**762.8**	**8.1**	rel to 28.201 Ma FC
VM	ING01	10800+10801	sanidine+leucite	6/28	649.3	3.8	0.3	Florindo et al., 2007	**653.4**	**3.8**	rel to 28.201 Ma FC
SC	R93-06N*	8281	sanidine	9/9	611	3		Karner and Renne, 1998	**614.9**	**3.0**	rel to 28.201 Ma FC
SC	R95-06A*	30181	sanidine	5/5	607	6		Karner and Renne, 1998	**610.9**	**6.0**	rel to 28.201 Ma FC
FAD 0	FoMF-C1	33154	sanidine	6/6	^591	6	0.6	Marra et al., 2009	**594.8**	**6.1**	rel to 1.201 Ma ACS
FAD 0	AH20-C6	11378	sanidine	5/6	587	3		Marra et. al., 2009	**590.7**	**3.0**	rel to 28.201 Ma FC
FAD 0	ING-02	10804+10805	sanidine+leucite	10/12	582	3	1.9	Florindo et al., 2007	**585.7**	**3.0**	rel to 28.201 Ma FC
FAD-2 rwd	R93-25A-1†	7588	sanidine	4/6	561	3		Karner and Renne, 1998	**564.6**	**3.0**	rel to 28.201 Ma FC
LTGVT	R93-25A-2†	7588	sanidine	2/6	545	8		Karner and Renne, 1998	**548.5**	**8.1**	rel to 28.201 Ma FC
UTGVT	R93-02	7589	sanidine	7/7	542	3		Karner and Renne, 1998	**545.5**	**3.0**	rel to 28.201 Ma FC
UTGVT	CAL03-05-06	11072+76+85	sanidine	18/20	548	10		Karner et al., 2001	**551.5**	**10.1**	rel to 28.201 Ma FC
SdC	SdC	-	?	?	520	10		Gaeta et al., 2003	**523.3**	**10.1**	rel to 28.201 Ma FC
TGPP	LAB-01	11095	sanidine	4/7	514	5		Karner et al., 2001	**517.3**	**5.0**	rel to 28.201 Ma FC
GRPS-a	PAL-01**	11100	sanidine	5/5	516	6		Karner et al., 2001	**519.3**	**6.0**	rel to 28.201 Ma FC
GRPS-b	SAX-01**	11082	sanidine	5/5	508	9		Karner et al., 2001	**511.2**	**9.1**	rel to 28.201 Ma FC
GRPS	R93-22C	7582	sanidine	7/7	500	6		Karner and Renne, 1998	**506.5**	**6.0**	rel to 28.201 Ma FC
GRPS	CR1	33150	sanidine	5/5	507	4	0.7	previuosly unpublished	**510.2**	**4.1**	rel to 28.201 Ma FC
FALL A1 up	CR5	33151	sanidine	8/8	496	3	1.4	previously unpublished	**499.2**	**3.0**	rel to 28.201 Ma FC
FALL B	R93-11M***	7577	sanidine	9/9	487	4	3.3	Karner and Renne, 1998	**490.1**	**4.1**	rel to 28.201 Ma FC
TRSN	R93-26A	7583	sanidine	9/9	449	2		Karner and Renne, 1998	**451.9**	**2.0**	rel to 28.201 Ma FC
rwd	R94-22b	8299	sanidine	8/8	462	7		Karner and Renne, 1998	**465.0**	**7.0**	rel to 28.201 Ma FC
rwd	R95-04H	30175	sanidine	3/3	437	8		Karner and Renne, 1998	**439.8**	**8.1**	rel to 28.201 Ma FC
VICO ?	R94-30C**	8292	sanidine	7/7	422	5		Karner and Renne, 1998	**427.4**	**5.0**	rel to 28.201 Ma FC
VICO	SPQR-51	7108	sanidine	7/7	416	11		Karner et al., 2001	**418.7**	**11.1**	rel to 28.201 Ma FC
VICO	C7	10811	sanidine	8/8	410	2		Karner et al., 2001	**412.3**	**2.0**	rel to 28.201 Ma FC

40Ar/39Ar ages from previous works. The ages in the sixth column are the original mean weighted ages calculated according to 28.02 Ma for the Fish Canyon Tuff sanidine or, those marked ^, to 1.194 Ma for the Alder Creek Tuff sanidine. The number of analyses refers to the data included in the mean weighted age with respect to the total number of dated crystal for each sample. All the analyses included in this table are on single crystal. The criterion of exclusion is a 2σ cutoff, with the exception of the sample marked † for which two mean weighted ages are computed on two populations of crystals overlapping at 2σ. Mean weighted ages for samples marked * have been re-calculated in Marra and Florindo (submitted) from original datasheet in Karner and Renne (1998); those marked ** have been recalculated here from original data; full Ar/Ar data in Appendix 3.
Sample marked *** was re-processed along with samples CR1 and CR5 from the same sampling site, using the same data reduction method; full Ar/Ar data in Appendix 2.
LEGEND: PT: Paleotiber Succession; PG: Ponte Galeria Eruption Unit; VM: Vigna Murata Eruption Unit; SC: Santa Cecilia Eruption Unit; TGCP: Tufo Giallo di Castelnuovo di Porto; FAD: First Ashfall Deposit; LTGVT: Lower Tufo Giallo della Via Tiberina; UTGVT: Upper Tufo Giallo della Via Tiberina; SdC: Sella di Corno; TGPP: Tufo Giallo di Prima Porta; GRPS: Grottarossa Pyroclastic Sequence; TRSN: Tufo Rosso a Scorie Nere; rwd: reworked.

Table 4

Table 4 Electron microprobe analyses of glasses occurring in the studied pyroclasts

Unit	**Morlupo spatter**		**TGCP**		**TGCP**		**FAD-2**		**FAD 3A**		**TGPP**	
Type	**WP**		**WP**		**GP**		**GP**		**WP**		**WP**	
Sample/ locality	**MG8-**		**FDC1 middle**		**FDC1 upper Lct-bearing glass**		**Fall PG**		**FAD2**		**MG12 Cava Vicoli**	
	(6)[a]	*σ*	*(7)*	*σ*	*(8)*	*σ*	*(3)*	*σ*	*(3)*	*σ*	*(6)*	*σ*
SiO_2	53.43	*1.16*	53.53	*1.00*	52.39	*1.26*	56.23	*0.80*	53.64	*1.08*	53.61	*0.65*
TiO_2	0.26	*0.02*	0.52	*0.05*	0.80	*0.12*	0.47	*0.05*	0.24	*0.03*	0.38	*0.05*
Al_2O_3	20.03	*0.38*	18.97	*0.41*	17.63	*0.93*	18.57	*0.30*	20.52	*0.75*	19.20	*0.16*
FeO	2.21	*0.11*	3.88	*0.31*	5.63	*0.99*	2.91	*0.09*	2.10	*0.28*	2.62	*0.09*
MnO	0.22	*0.04*	0.25	*0.07*	0.27	*0.05*	0.16	*0.01*	0.19	*0.11*	0.19	*0.05*
MgO	0.18	*0.02*	0.59	*0.08*	1.53	*0.66*	0.44	*0.04*	0.18	*0.04*	0.23	*0.02*
CaO	3.03	*0.23*	5.73	*0.71*	8.43	*1.44*	2.81	*0.10*	3.16	*0.65*	3.44	*0.09*
Na_2O	4.82	*0.14*	5.32	*0.31*	4.67	*0.35*	3.00	*0.18*	6.65	*0.91*	3.80	*0.15*
K_2O	9.29	*0.20*	5.68	*0.58*	3.75	*0.34*	10.07	*0.22*	4.85	*1.50*	9.85	*0.33*
P_2O_5	0.03	*0.02*	0.17	*0.27*	0.20	*0.05*	0.05	*0.03*	0.04	*0.01*	0.03	*0.02*
SO_2	0.15	*0.05*	0.35	*0.09*	0.28	*0.06*	0.00	*0.00*	0.18	*0.08*	0.21	*0.03*
F	0.63	*0.09*	0.61	*0.09*	0.60	*0.12*	0.00	*0.00*	0.78	*0.36*	0.38	*0.08*
Cl	0.17	*0.19*	0.11	*0.02*	0.10	*0.04*	0.10	*0.04*	0.10	0.02	0.09	*0.01*
Total	94.46		95.71		96.27		94.82		92.63		94.02	

WP: white pumice; GP: grey pumice; Lct: leucite; a: number of point analyses used in the average and standard deviation *(σ)*.

Table 4 (continued)

Unit	GRPS-d		FALL A		FALL A		FALL B1		Fall C	Fall D	
Type	MI in BS Cpx		WP		WP		WP		MI in Cpx of BS	MI in Cpx of WP	
Sample	Mg13		Fall a GR		Fall a VT		Fall b			SPX33	
	(5)[a]	σ	(5)	σ	(6)	σ	(4)	σ	(2)	(3)	σ
SiO_2	46.47	1.64	55.75	0.73	56.23	0.33	55.05	0.88	49.11	57.46	0.90
TiO_2	0.67	0.11	0.48	0.02	0.46	0.02	0.44	0.01	1.18	0.62	0.13
Al_2O_3	17.98	0.39	17.89	0.21	18.02	0.07	17.44	0.29	17.39	18.76	0.84
FeO	6.48	1.17	2.88	0.08	3.03	0.12	2.65	0.06	7.72	3.29	0.46
MnO	0.14	0.07	0.15	0.03	0.17	0.13	0.14	0.02	0.38	0.21	0.03
MgO	1.90	0.98	0.47	0.02	0.49	0.06	0.46	0.04	0.63	0.22	0.12
CaO	7.88	0.59	3.16	0.24	2.84	0.08	3.01	0.17	8.79	3.20	1.08
Na_2O	1.78	0.37	2.96	0.13	2.76	0.14	2.89	0.18	3.25	2.35	1.39
K_2O	9.77	1.17	9.52	0.14	9.55	0.25	9.49	0.23	7.12	10.34	0.77
P_2O_5	1.10	0.11	0.09	0.04	0.07	0.01	0.05	0.01	0.06	0.23	0.25
SO_2	0.74	0.30	0.29	0.40	0.19	0.04	0.16	0.02	0.30	0.27	0.09
F	0.31	0.09	0.31	0.11	0.33	0.08	0.24	0.11	0.48	0.21	0.27
Cl	0.07	0.03	0.12	0.03	0.10	0.02	0.12	0.03	0.10	0.05	0.04
Total	95.28		94.06		94.22		92.14		96.51	97.22	

WP: white pumice; MI: melt inclusion; Cpx: clinopyroxene; a: number of point analyses used in the average and in the standard deviation *(σ)*.

Table 4 (continued)

Unit	TRSN (basal fallout)		TRSN (piroclastic flow)		Fall E		Fall E		Fall E		Fall F	
Type	WP		BP		MI in Cpx		WP		WP		MI in Cpx of GS	
Sample/ locality	Isola Farnese				SPX35		Prima Porta		S. Abbondio		SPX37	
	(18)[a]	σ	(25)	σ	(3)	σ	(11)	σ	(4)	σ	(4)	σ
SiO_2	56.18	1.21	59.30	0.95	56.37	0.57	57.49	0.53	56.58	0.77	47.43	0.30
TiO_2	0.49	0.04	0.50	0.03	0.49	0.05	0.49	0.08	0.35	0.13	0.73	0.03
Al_2O_3	17.89	0.17	18.21	0.28	17.79	0.06	18.27	0.41	19.34	0.62	17.66	0.02
FeO	2.74	0.10	2.57	0.13	2.86	0.24	2.50	0.16	2.30	0.15	6.83	0.14
MnO	0.14	0.03	0.16	0.04	0.14	0.01	0.12	0.03	0.20	0.05	0.14	0.01
MgO	0.38	0.02	0.37	0.03	0.47	0.13	0.35	0.07	0.26	0.04	3.79	0.08
CaO	2.63	0.11	2.57	0.28	2.66	0.14	2.52	0.11	2.40	0.23	8.07	0.24
Na_2O	3.52	0.09	3.34	0.45	2.49	0.15	3.43	0.21	5.24	0.33	2.03	0.08
K_2O	9.56	0.10	9.77	0.66	9.70	0.32	9.57	0.39	8.59	0.12	8.37	0.14
P_2O_5	0.05	0.03	0.05	0.03	0.04	0.04	0.05	0.03	0.01	0.02	0.50	0.02
SO_2	0.00	0.00	0.14	0.06	0.27	0.01	0.07	0.07	0.00	0.00	0.66	0.02
F	0.33	0.10	0.21	0.15	0.32	0.13	0.14	0.17	0.00	0.00	0.30	0.09
Cl	0.08	0.01	0.07	0.02	0.06	0.01	0.09	0.02	0.15	0.04	0.06	0.02
Total	93.58		96.84		93.66		95.09		95.42		96.57	

WP: white pumice; BP: black pumice; MI: melt inclusion; Cpx: clinopyroxene; GS: grey scoria; a: number of point analyses used in the average and in the standard deviation *(σ)*.

Table ? (continued)

Unit	Vico α		Vico α		Vico β		Vico β	
Type	WP		WP		WP		WP	
Sample/ locality	II Fall S. Abbondio		San Martino		San Martino		III Fall S. Abbondio	
	(4)[a]	*σ*	*(4)*	*σ*	*(4)*	*σ*	*(4)*	*σ*
SiO_2	69.27	*0.84*	68.01	*0.40*	54.25	*0.19*	55.63	*1.21*
TiO_2	0.22	*0.09*	0.22	*0.07*	0.51	*0.14*	0.53	*0.08*
Al_2O_3	14.37	*0.34*	14.28	*0.35*	19.77	*0.20*	19.36	*0.89*
FeO	1.27	*0.11*	1.23	*0.12*	3.32	*0.11*	3.24	*0.28*
MnO	0.06	*0.08*	0.10	*0.03*	0.09	*0.06*	0.20	*0.09*
MgO	0.08	*0.04*	0.10	*0.01*	0.31	*0.06*	0.30	*0.07*
CaO	1.20	*0.10*	1.17	*0.05*	4.15	*0.37*	4.17	*0.51*
Na_2O	3.35	*0.23*	3.29	*0.18*	4.37	*0.38*	5.38	*0.46*
K_2O	6.73	*0.15*	6.71	*0.30*	8.91	*0.70*	7.23	*0.46*
P_2O_5	0.00	*0.01*	0.02	*0.02*	0.03	*0.05*	0.04	*0.02*
SO_2	0.00	*0.00*	0.00	*0.00*	0.00	*0.00*	0.00	*0.00*
F	0.00	*0.00*	0.00	*0.00*	0.00	*0.00*	0.00	*0.00*
Cl	0.14	*0.01*	0.15	*0.02*	0.09	*0.02*	0.08	*0.03*
Total	96.70		95.28		95.80		96.16	

WP: white pumice; GP: grey pumice; a: number of point analyses used in the average and in the standard deviation *(σ)*.

Table 5 - XRF analyses of juvenile clasts

unit	Morlupo spatter	GRPS breccia	FAD-1 upper	FAD-1 lower	GRPS
location	Morlupo	Morlupo	Capena	Capena	breccia
sample	MOR 01	MOR 11-DS	MG-27GP	MG-26GP	GRPS-DS
SiO2	61.12	48.63	57.87	58.94	49.23
TiO2	0.19	1.01	0.59	0.54	0.92
Al2O3	20.29	16.57	21.90	20.60	16.25
FeOtot	4.16	9.48	4.73	4.30	9.49
MgO	0.13	0.16	0.26	0.27	0.26
MnO	0.15	4.74	0.76	0.60	5.26
CaO	2.46	10.61	4.30	3.67	11.32
Na2O	3.81	0.61	4.79	5.81	4.69
K2O	7.70	7.80	4.64	5.13	1.83
P2O5	0.06	0.60	0.16	0.13	0.75
Total	100.00	100.00	100.00	100.00	100.00
LOI/EMP total	1.54	2.27	6.01	5.03	3.72

Table 6

TABLE 6 - Combined $^{40}Ar/^{39}Ar$ ages

1							
UNIT	SAMPLE	LAB. NUMBER	MINERAL	NUMBER OF ANALYSES	MEAN WEIGHTED AGE (ka)	Error (±2σ)	ORIGINAL REFERENCE
Paleotiber succession Unit B	I-9B+ PTS14-A	33180+33179 +33178	leucite+ sanidine	21/22	799.7	8.9	Florindo et al., 2007
Paleotiber succession Unit C	I9-A+ I7-A	33182+33181	sanidine	12/14	801.4	9.4	Florindo et al., 2007
Ponte Galeria Eruption Unit	R93-12F+ R95-16A	30189+ 7576	sanidine	9/21	760.0	6.2	Karner and Renne, 1998
Santa Cecilia Eruption Unit	R95-06N + R93-06A	30182+ 8281	sanidine	16/16	614.2	2.7	Karner and Renne, 1998
Grottarossa Pyroclastic Sequence (GRPS)	SAX-01+PAL-01+ CR1	11082+11100 +33150	sanidine	18/23	512.5	3.1	Karner et al., 2001a
2							
ERUPTIVE CYCLE	SAMPLE	AGES			MEAN WEIGHTED AGE (ka)	Error (±2σ)	
Prima Porta Eruptive Cycle (TGPP+GRPS)	SAX-01+PAL-01+ CR1+LAB01	511±9; 519±6; 510±4; 517±6			513.5	2.8	This work

Best eruption ages derived from the joined re-calculation of crystal ages from samples attributed to the same eruptive unit (1), or by combined weighted mean age of samples of the same eruptive cycle (2). All ages are calculated according to 28.201 Ma for the Fish Canyon Tuff sanidine.

*Figure 1

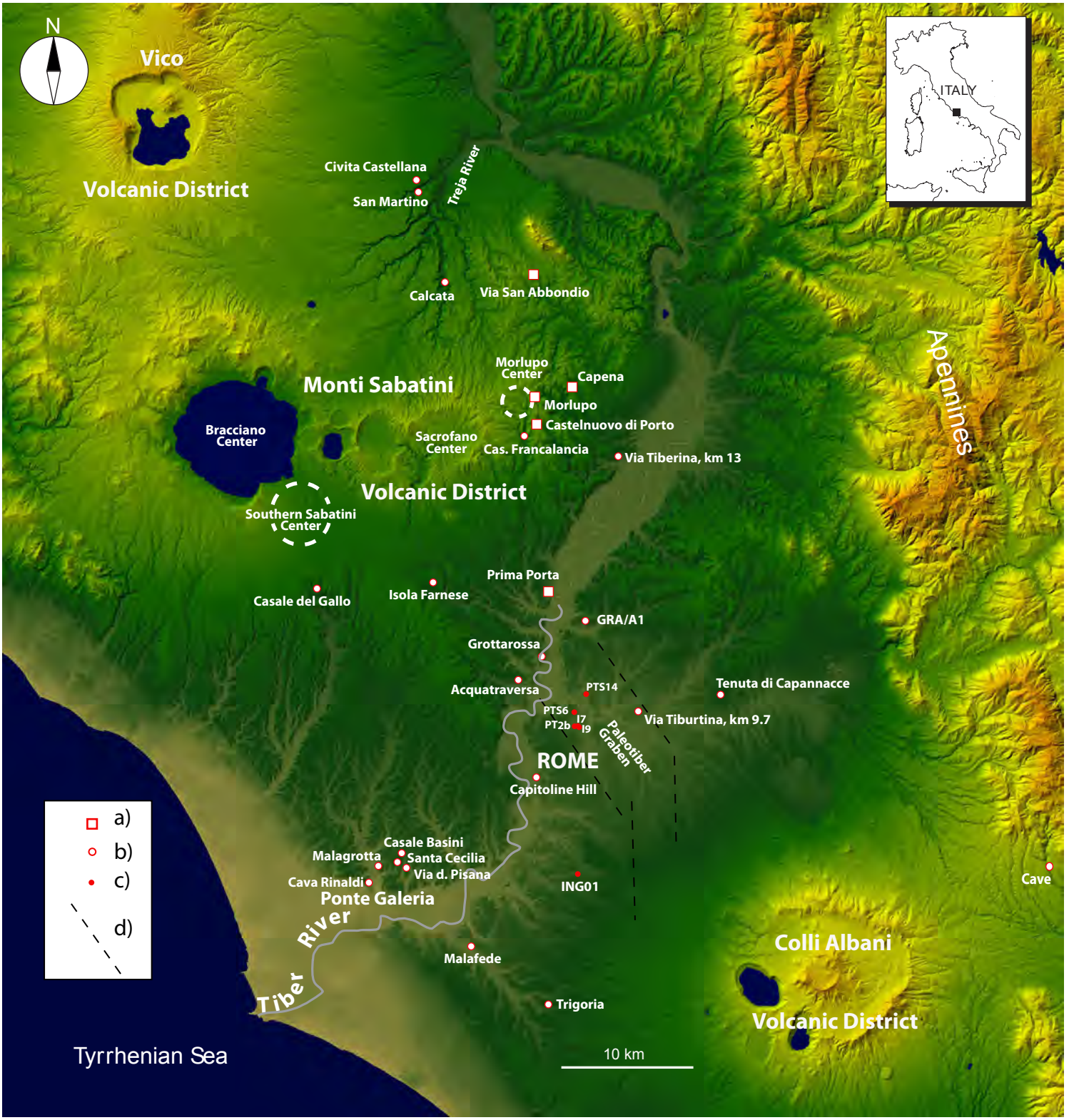

Figure 1

*Figure 2

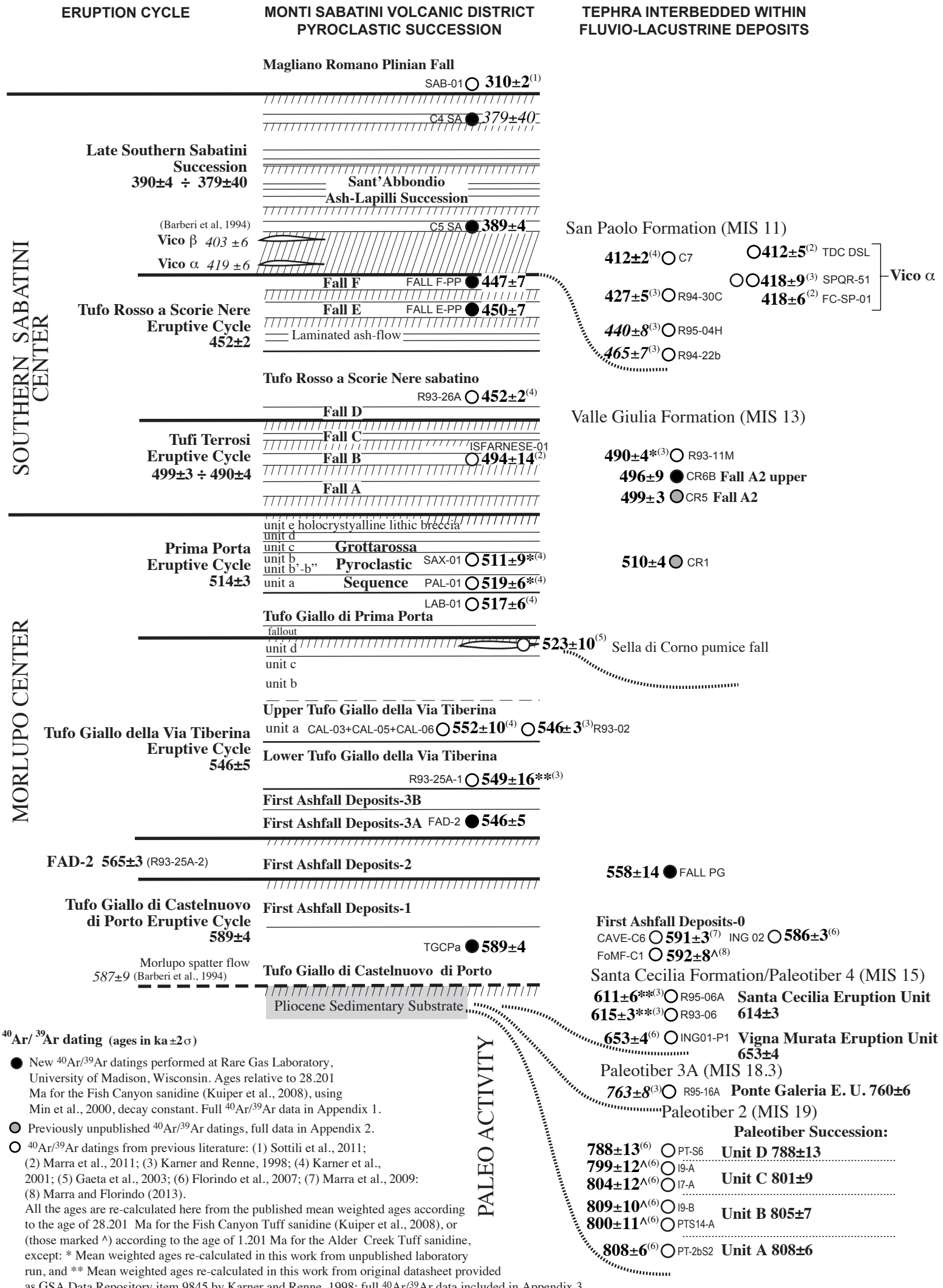

^{40}Ar/ ^{39}Ar dating (ages in ka ±2σ)

- ● New ^{40}Ar/^{39}Ar datings performed at Rare Gas Laboratory, University of Madison, Wisconsin. Ages relative to 28.201 Ma for the Fish Canyon sanidine (Kuiper et al., 2008), using Min et al., 2000, decay constant. Full ^{40}Ar/^{39}Ar data in Appendix 1.
- ◍ Previously unpublished ^{40}Ar/^{39}Ar datings, full data in Appendix 2.
- ○ ^{40}Ar/^{39}Ar datings from previous literature: (1) Sottili et al., 2011; (2) Marra et al., 2011; (3) Karner and Renne, 1998; (4) Karner et al., 2001; (5) Gaeta et al., 2003; (6) Florindo et al., 2007; (7) Marra et al., 2009: (8) Marra and Florindo (2013).

All the ages are re-calculated here from the published mean weighted ages according to the age of 28.201 Ma for the Fish Canyon Tuff sanidine (Kuiper et al., 2008), or (those marked ^) according to the age of 1.201 Ma for the Alder Creek Tuff sanidine, except: * Mean weighted ages re-calculated in this work from unpublished laboratory run, and ** Mean weighted ages re-calculated in this work from original datasheet provided as GSA Data Repository item 9845 by Karner and Renne, 1998; full ^{40}Ar/^{39}Ar data included in Appendix 3.

Figure 2

*Figure 3

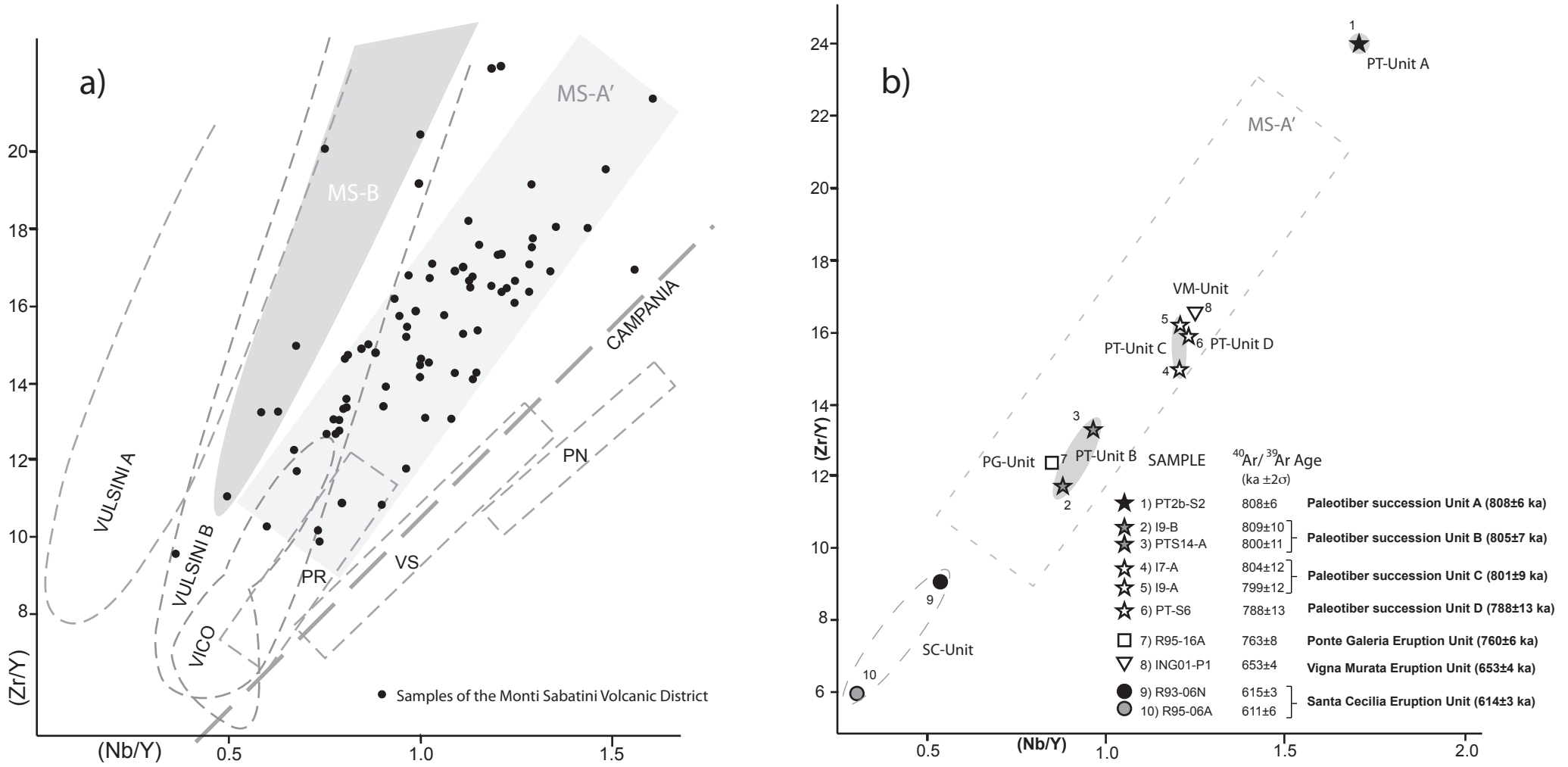

Figure 3

*Figure 4

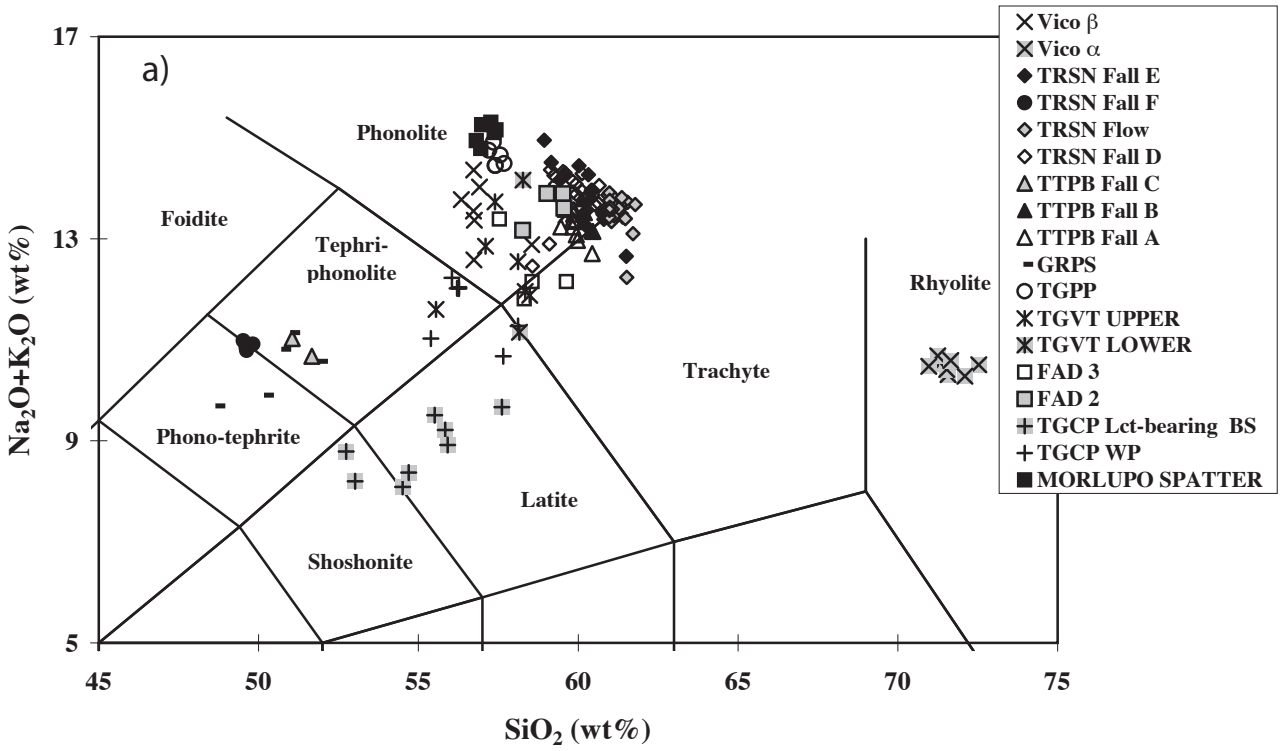

MORLUPO CENTER 589-517 ka

PRIMA PORTA ERUPTIVE CYCLE 517±6 ka
- GRPS (A) and TGPP (B) grey scoria
- TGPP white pumice

TGVT ERUPTIVE CYCLE 546±5 ka
- grey scoria
- white pumice
- FAD 3B grey scoria 546±5 ka
- FAD 3A white pumice 546±5 ka
- FAD 2 white pumice 558±14 ka

TGCP ERUPTIVE CYCLE 589±4 ka
- FAD 1 grey pumice
- TGCP grey pumice
- TGCP white pumice
- spatter flow
- white pumice in the spatter flow

SOUTHERN SABATINI CENTER 499-389 ka

SAA SUCCESSION 390±4 - 370±40 ka
- San Abbondio top dark grey scoria layer

TRSN ERUPTIVE CYCLE 452±2 ka
- FALL F grey scoria
- FALL E white pumice
- TRaSN black pumice
- Fall D white pumice

TT ERUPTIVE CYCLE 499±6 ka
- Fall C grey scoria
- Fall B grey scoria
- Fall B white pumice
- Fall A white pumice

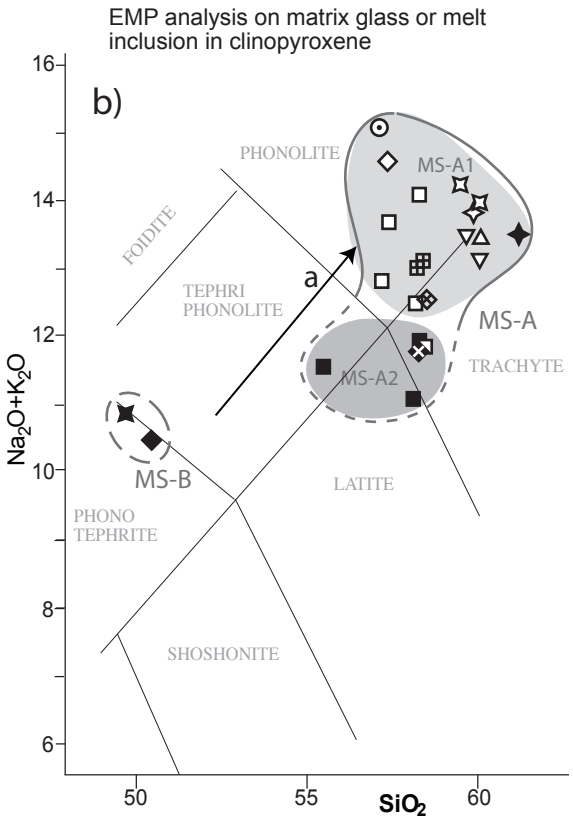

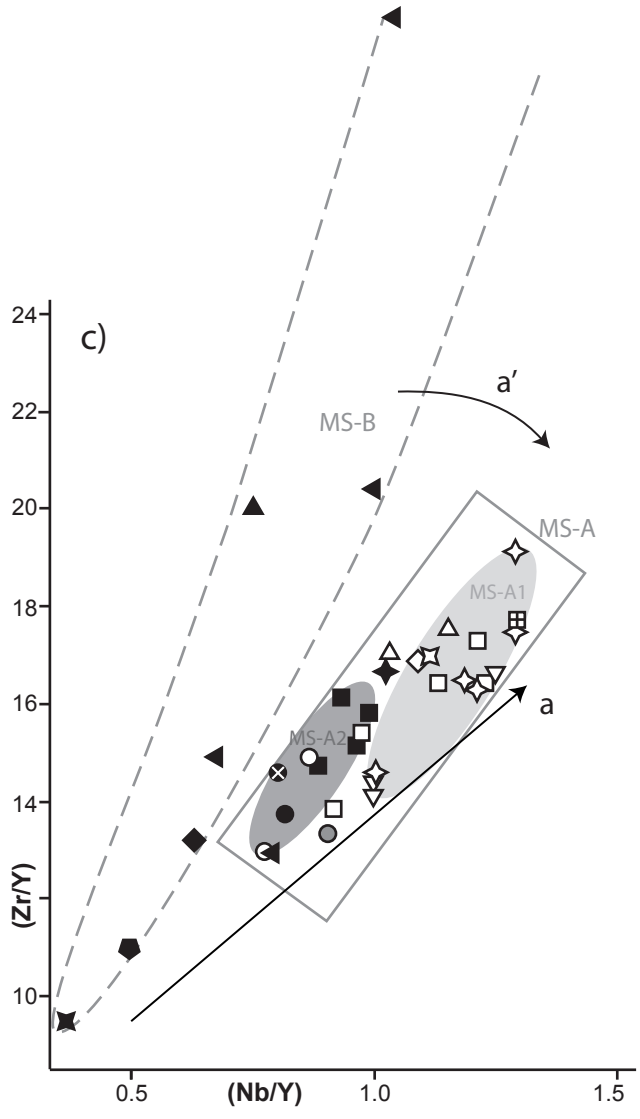

Figure 4

*Figure 5a

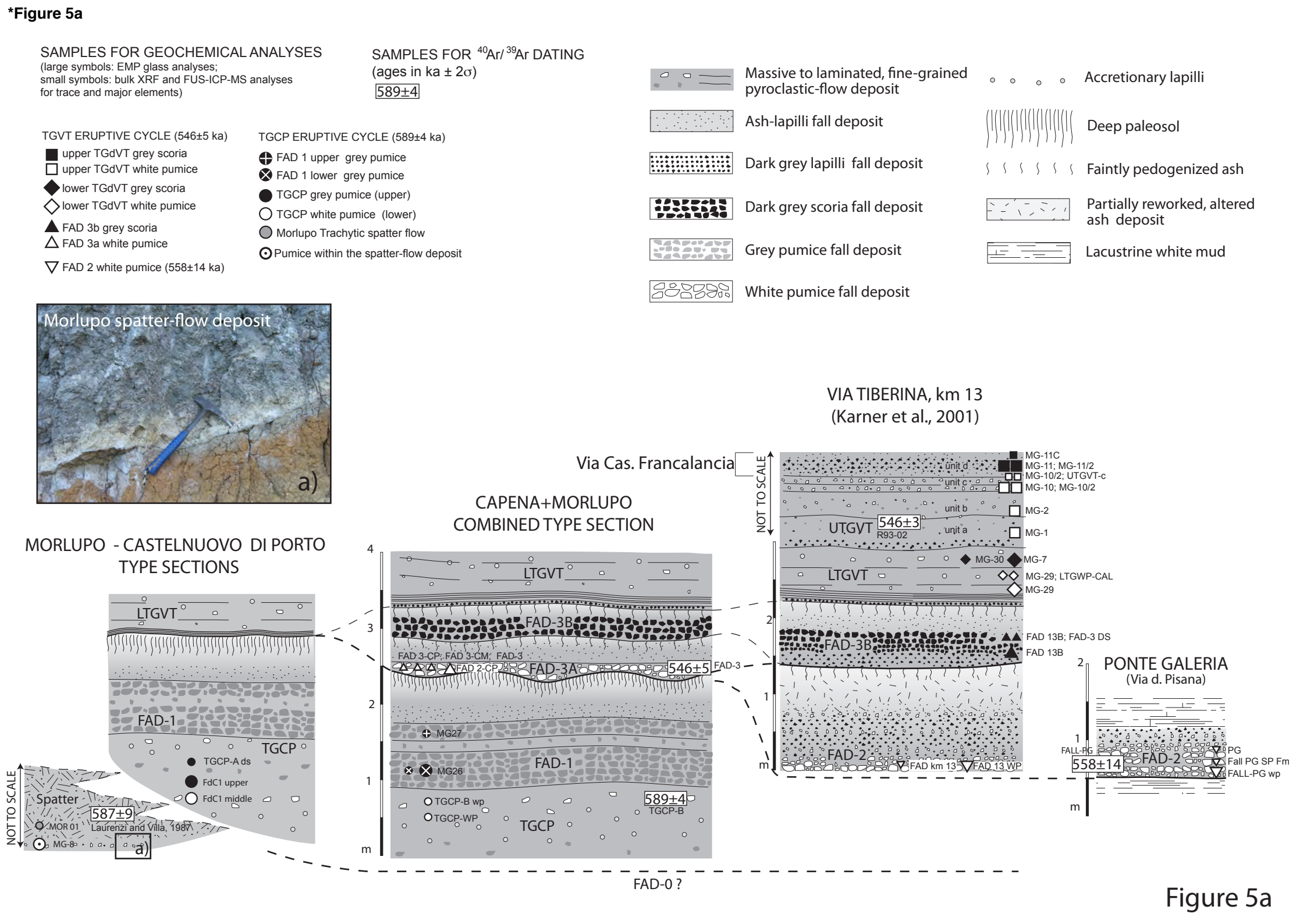

Figure 5a

*Figure 5b

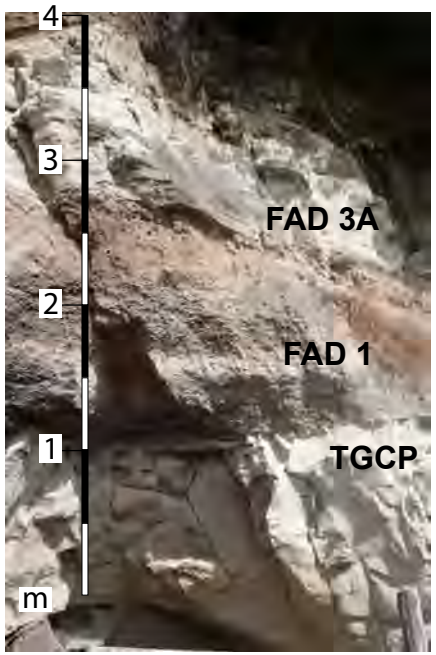

MORLUPO TYPE SECTION

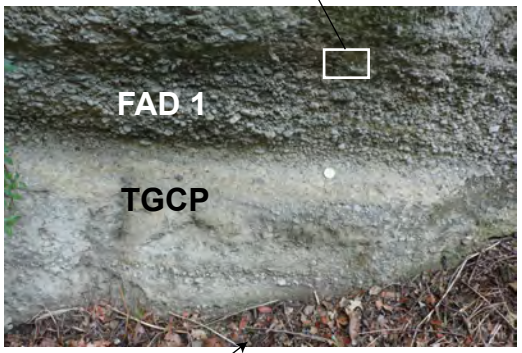

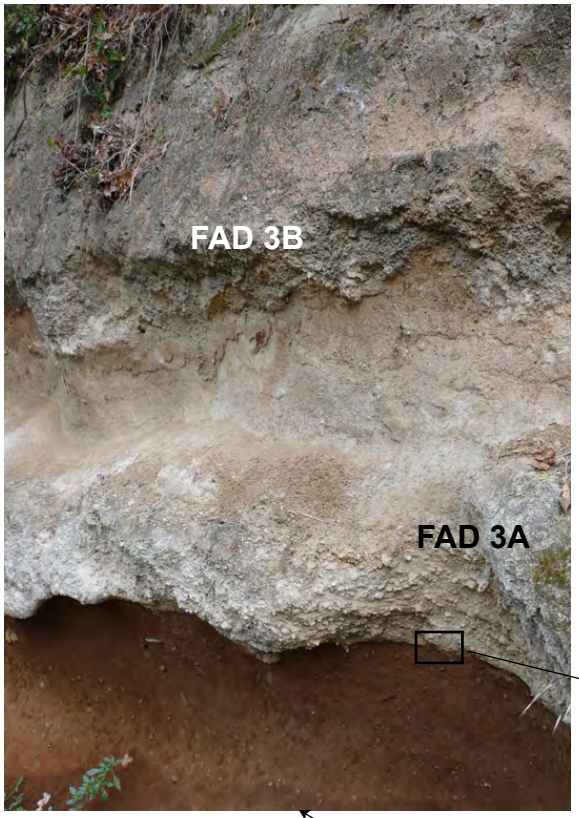

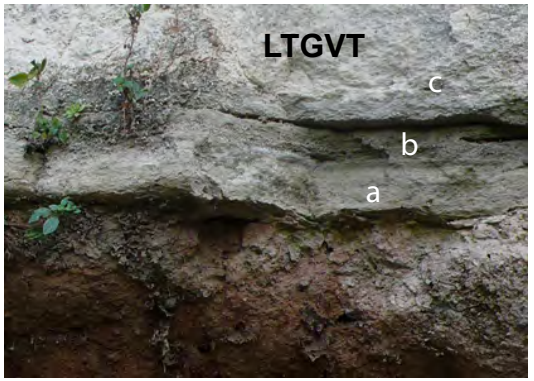

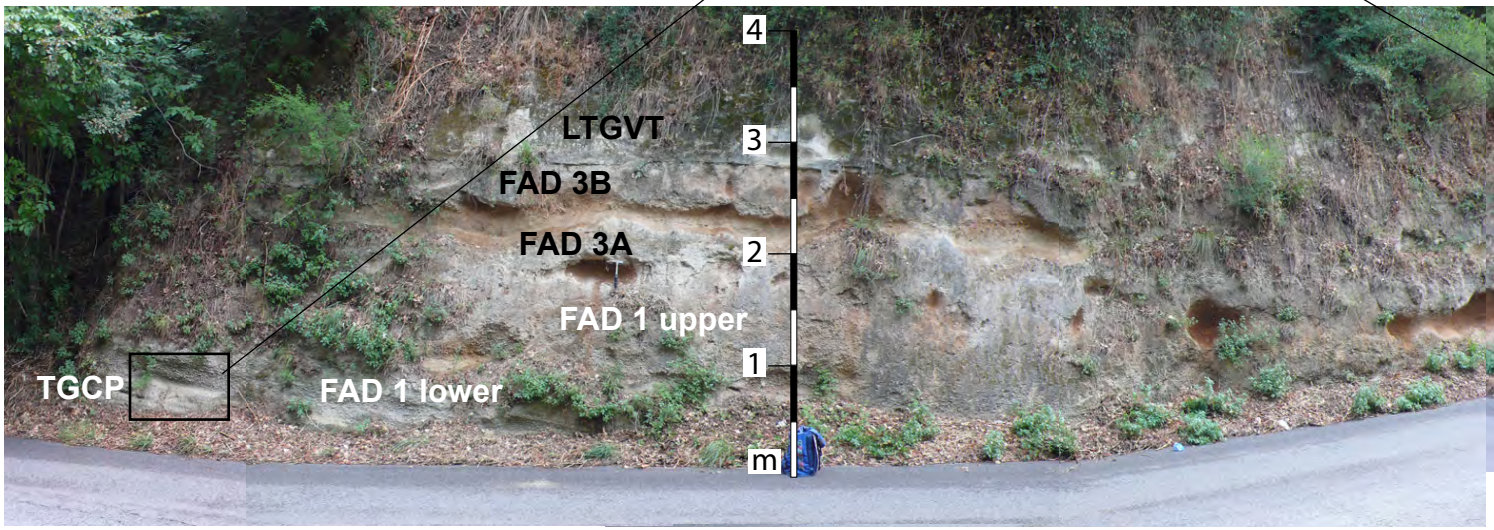

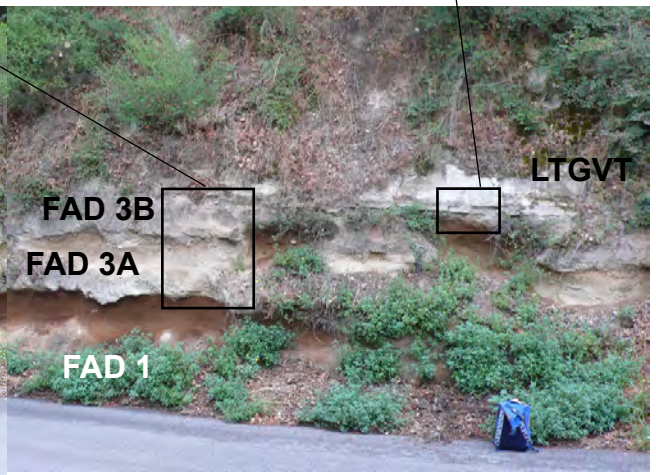

CAPENA TYPE SECTION

Figure 5b

*Figure 6

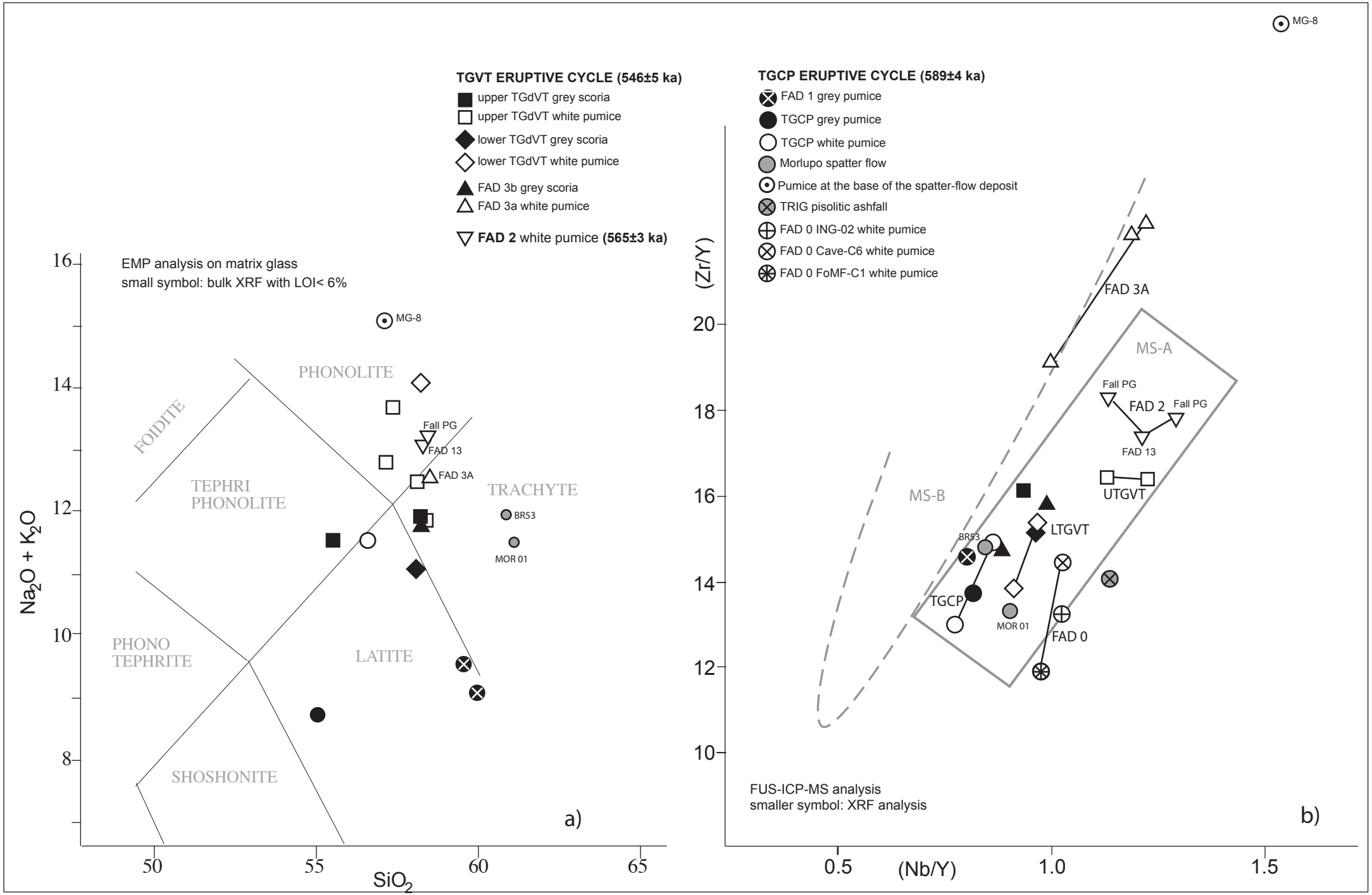

Figure 6

*Figure 7

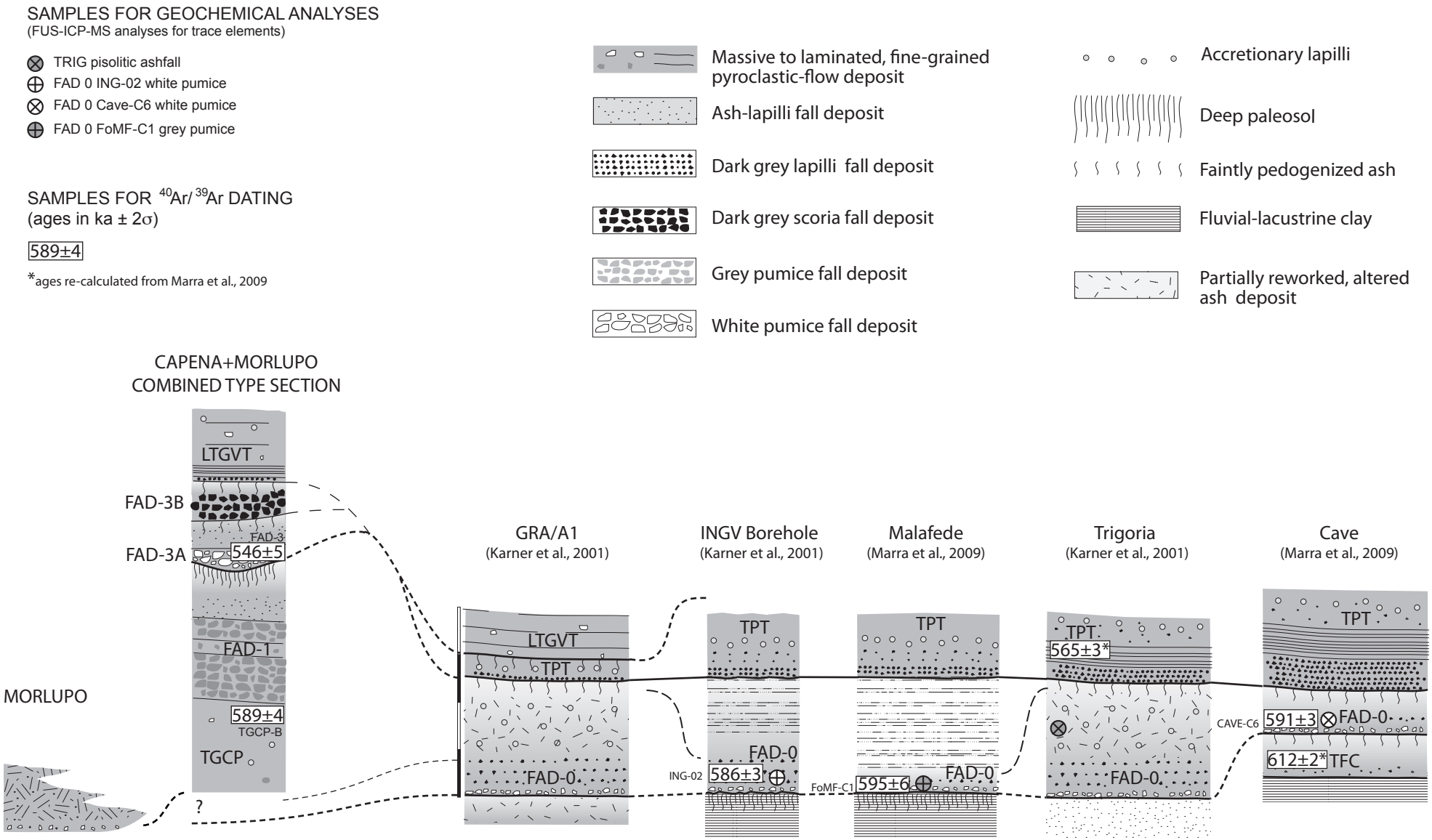

Figure 7

*Figure 8

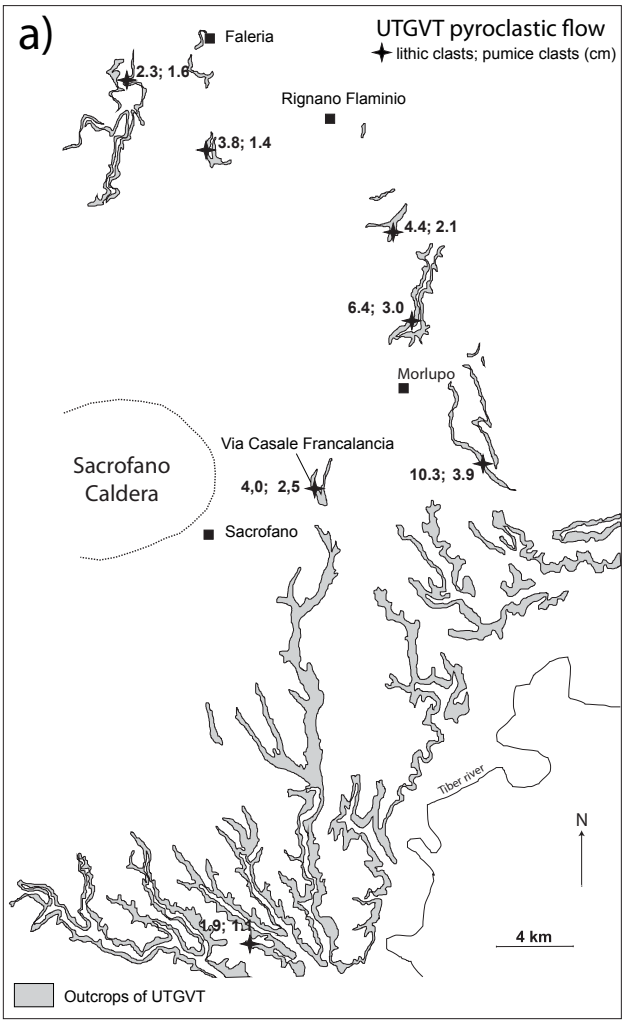

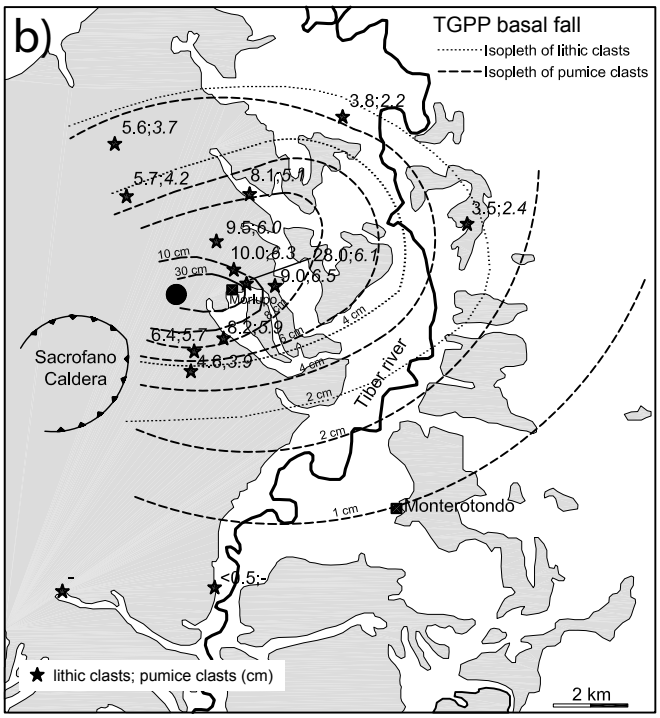

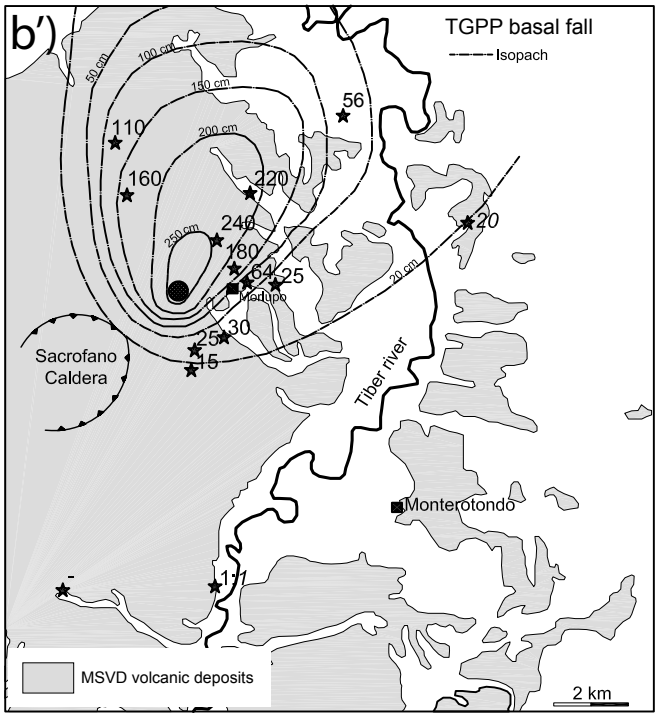

c) GRPS-e lithic breccia

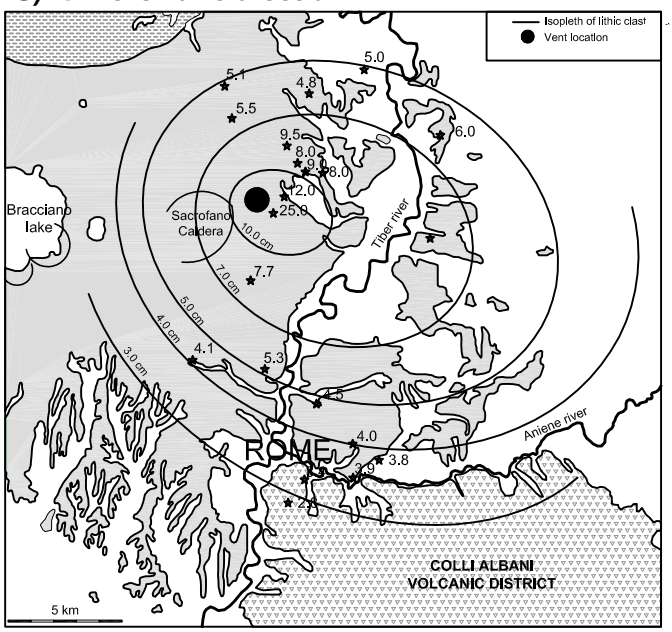

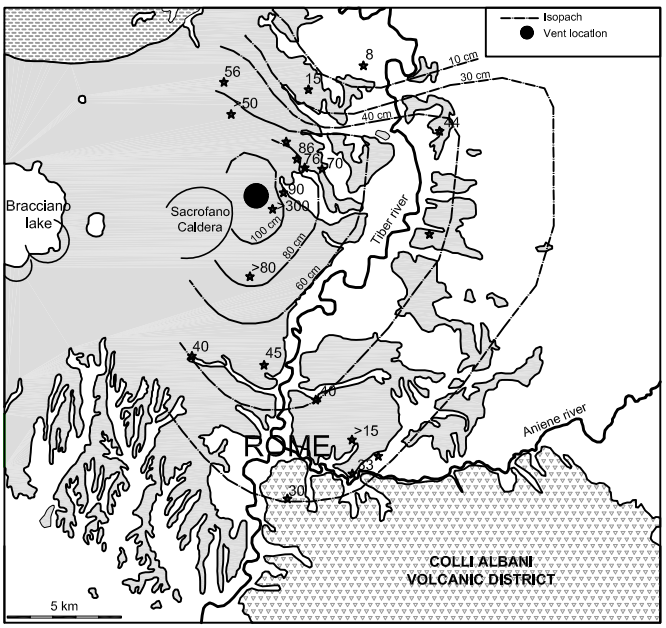

Figure 8

*Figure 9

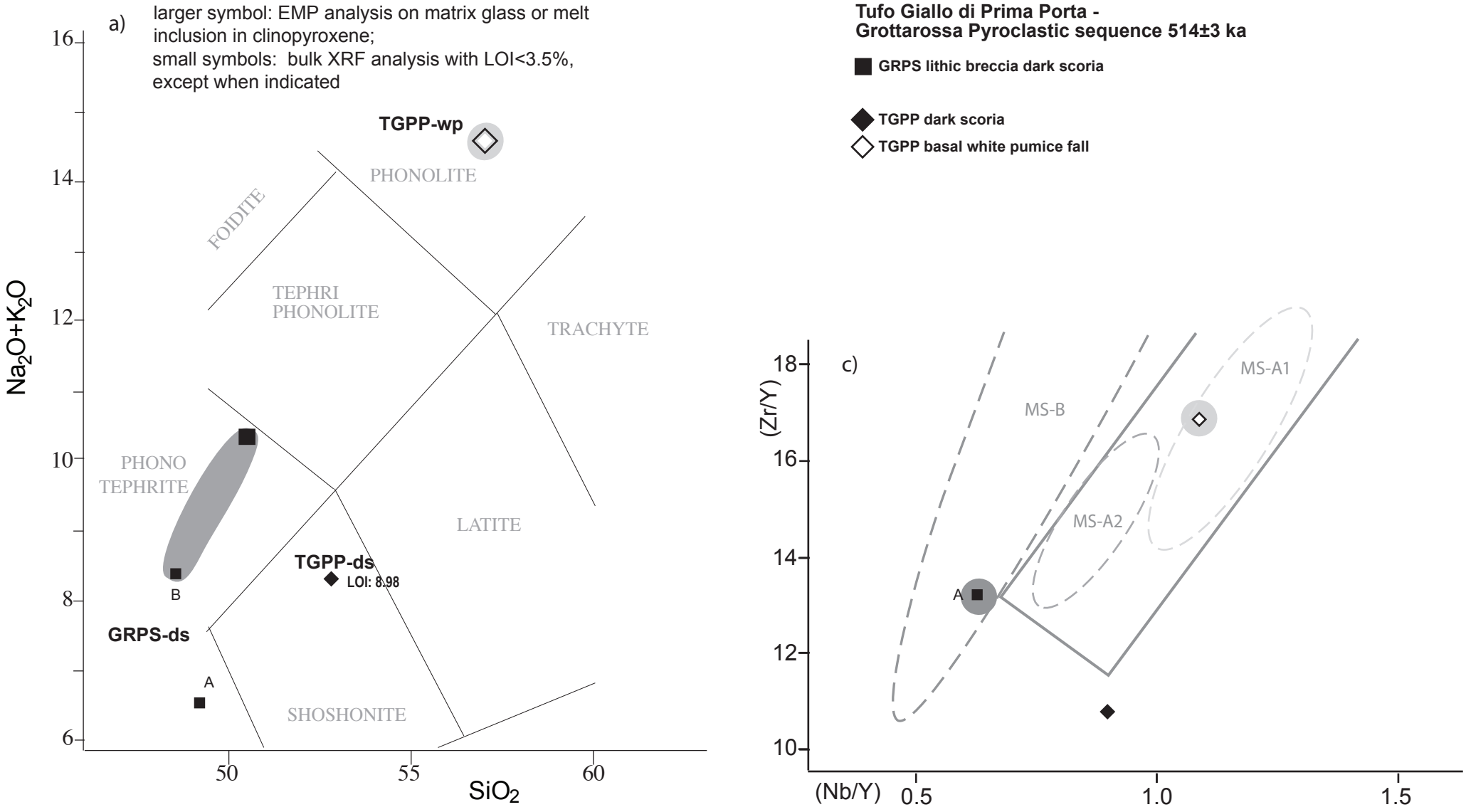

Figure 9

*Figure 10

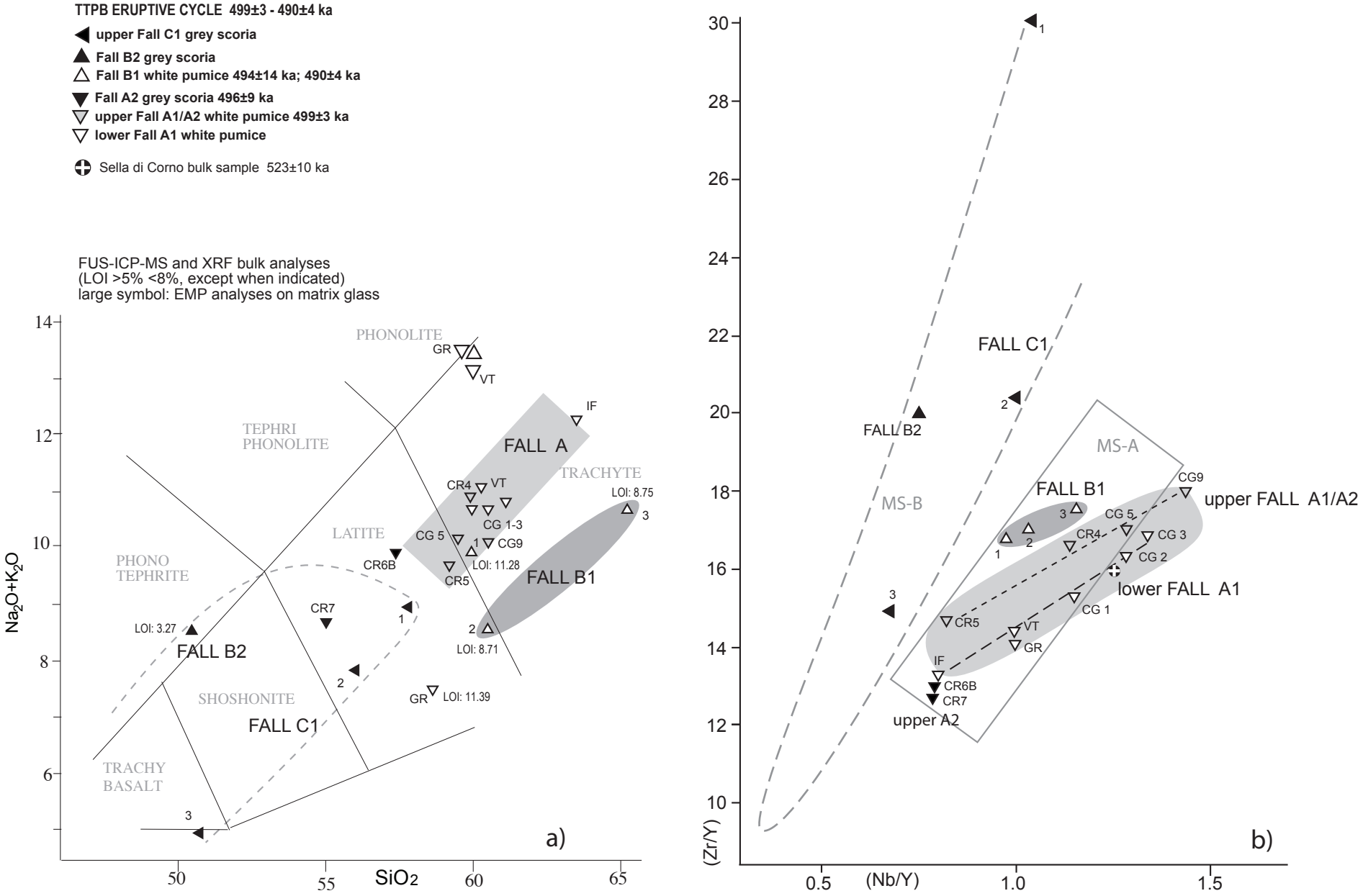

Figure 10

*Figure 11

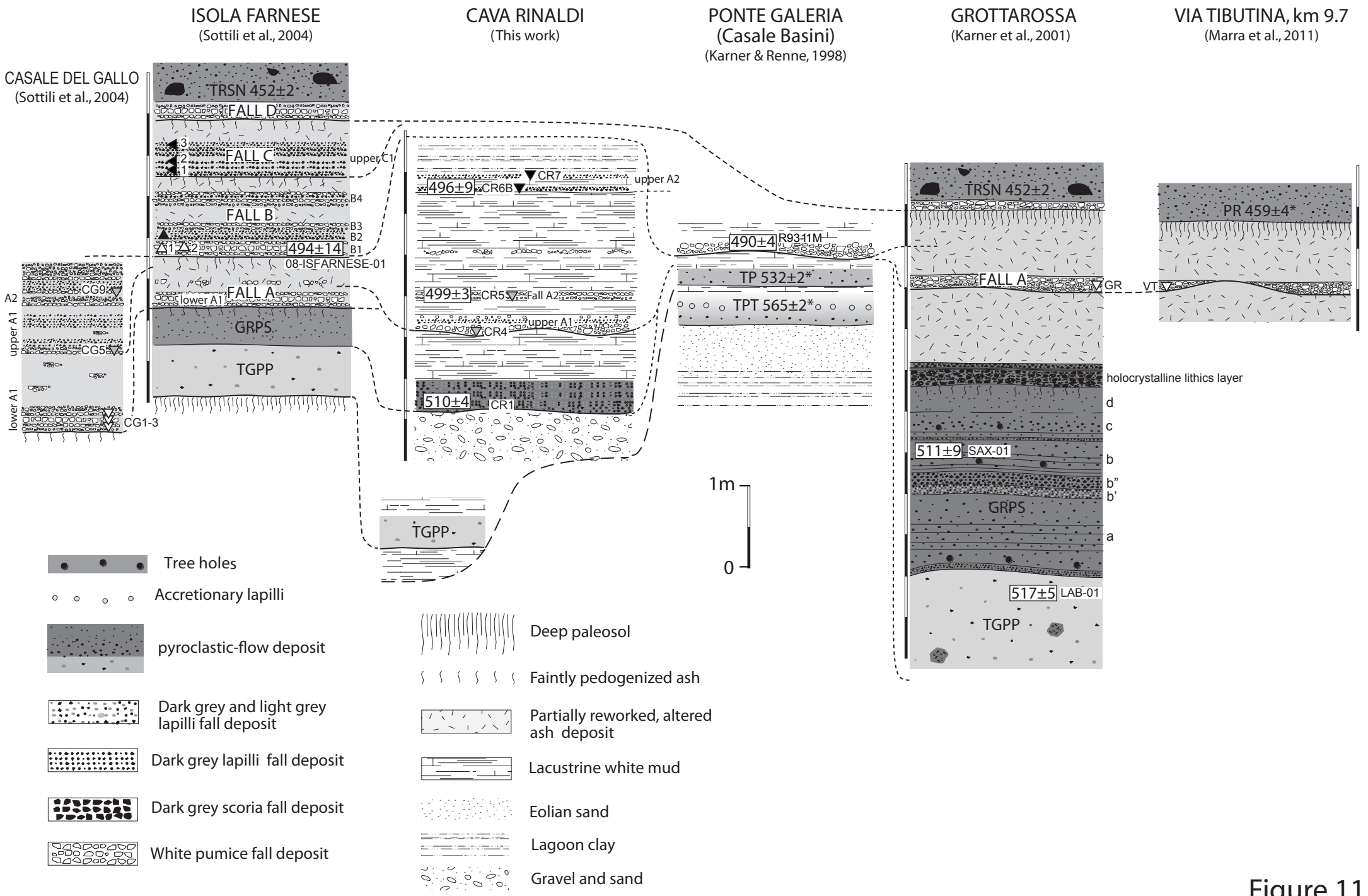

Figure 11

*Figure 12

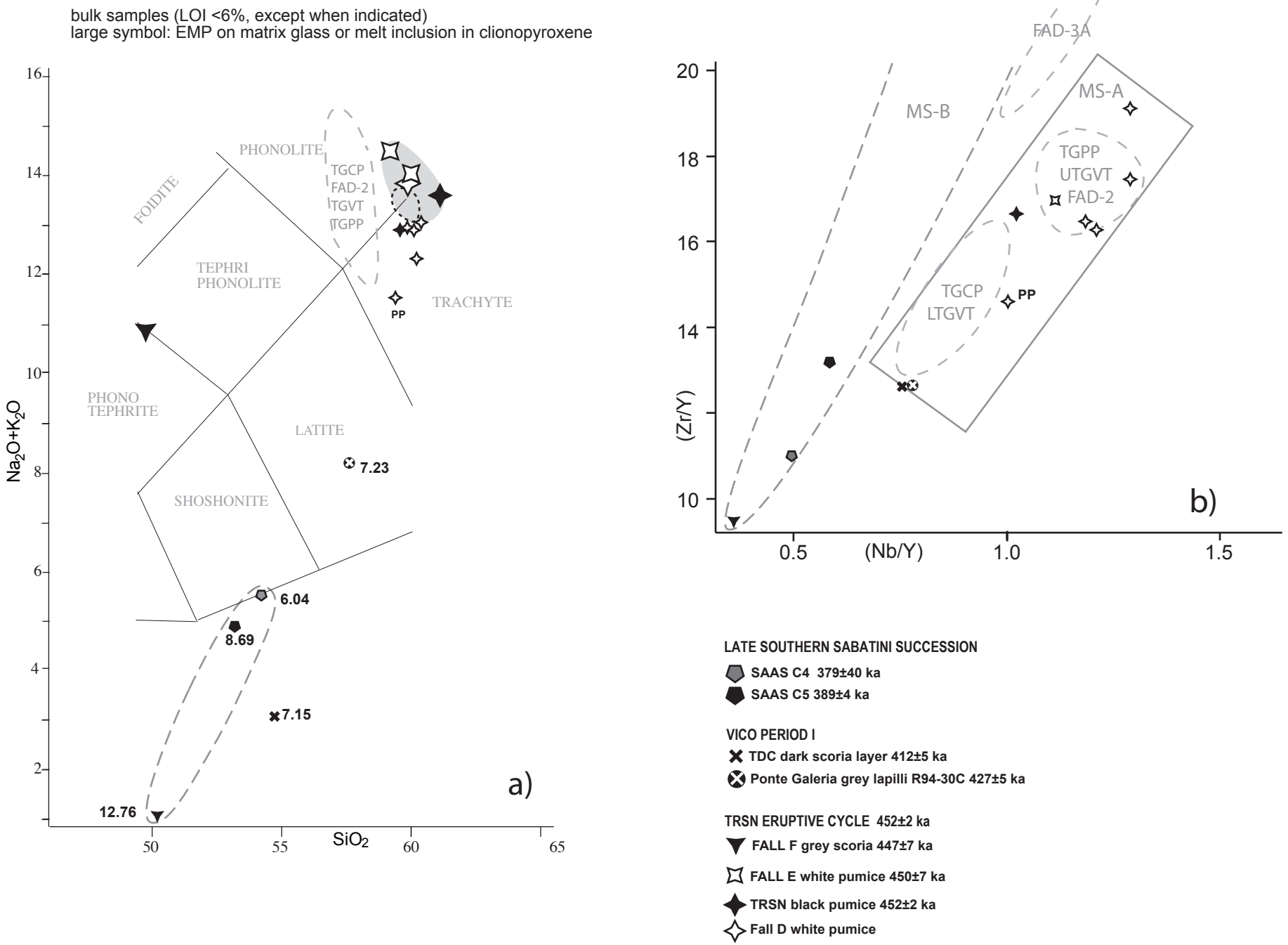

Figure 12

*Figure 13

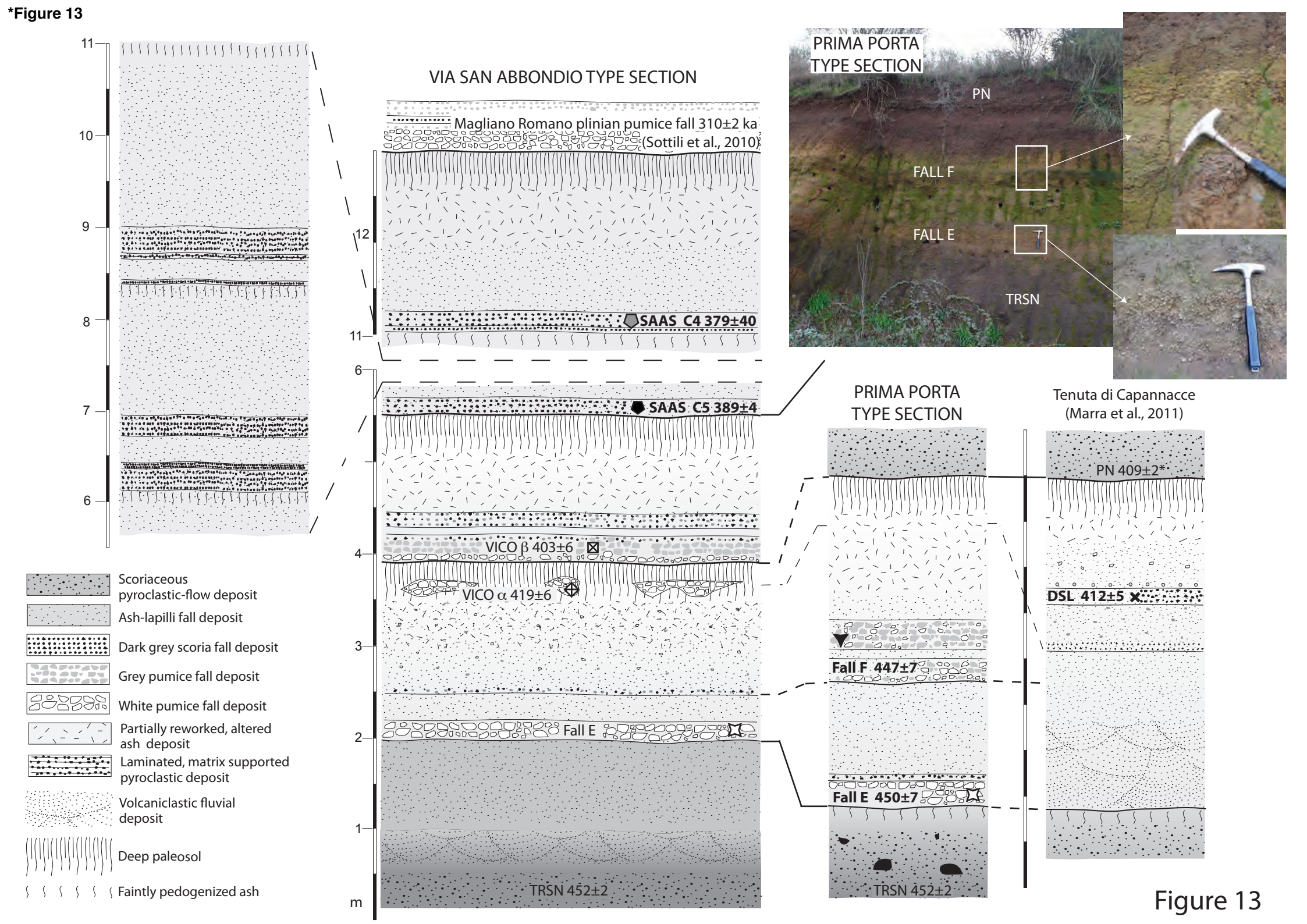

Figure 13

*Figure 14

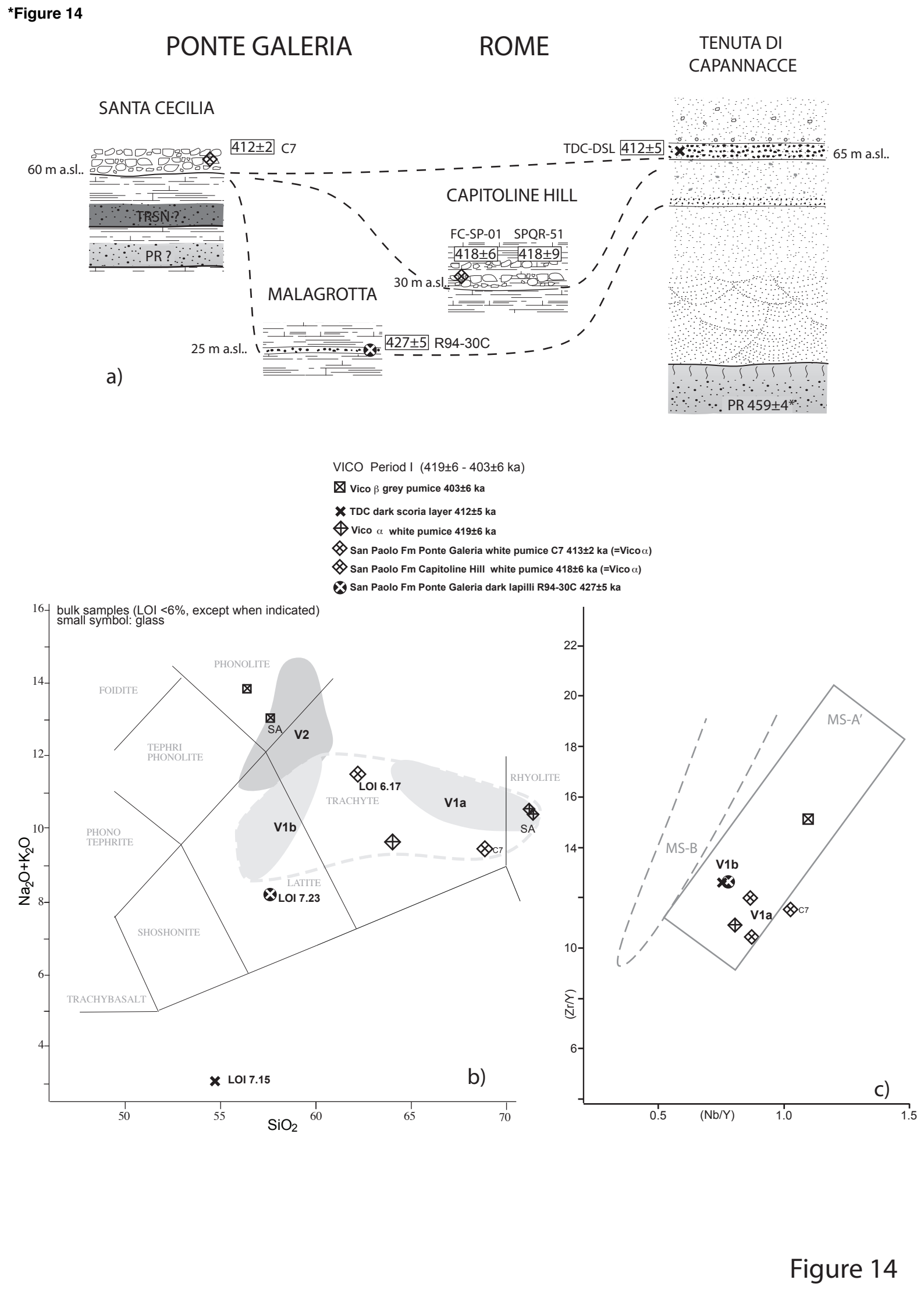

Figure 14

*Figure 15

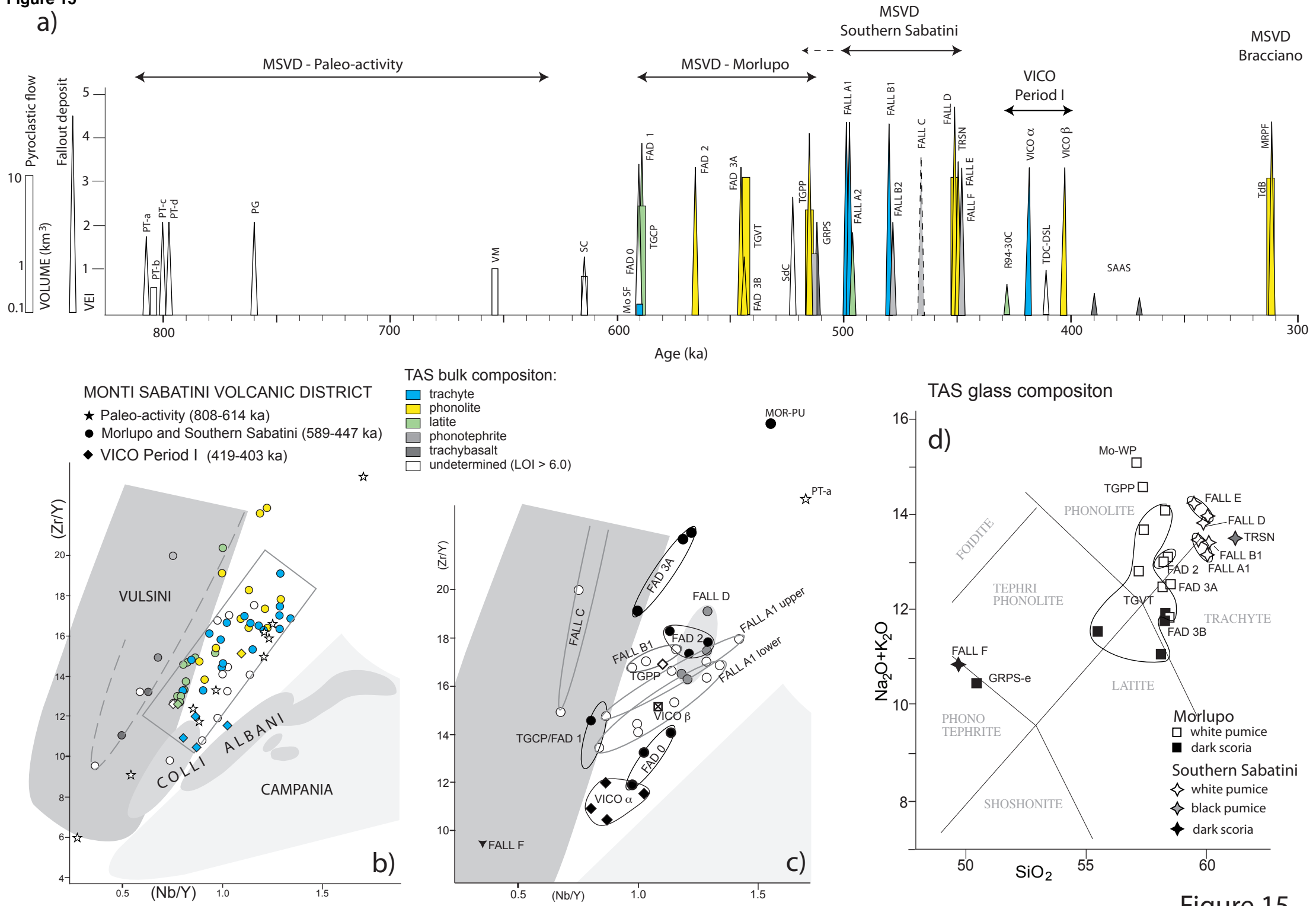

Figure 15

*Figure 16

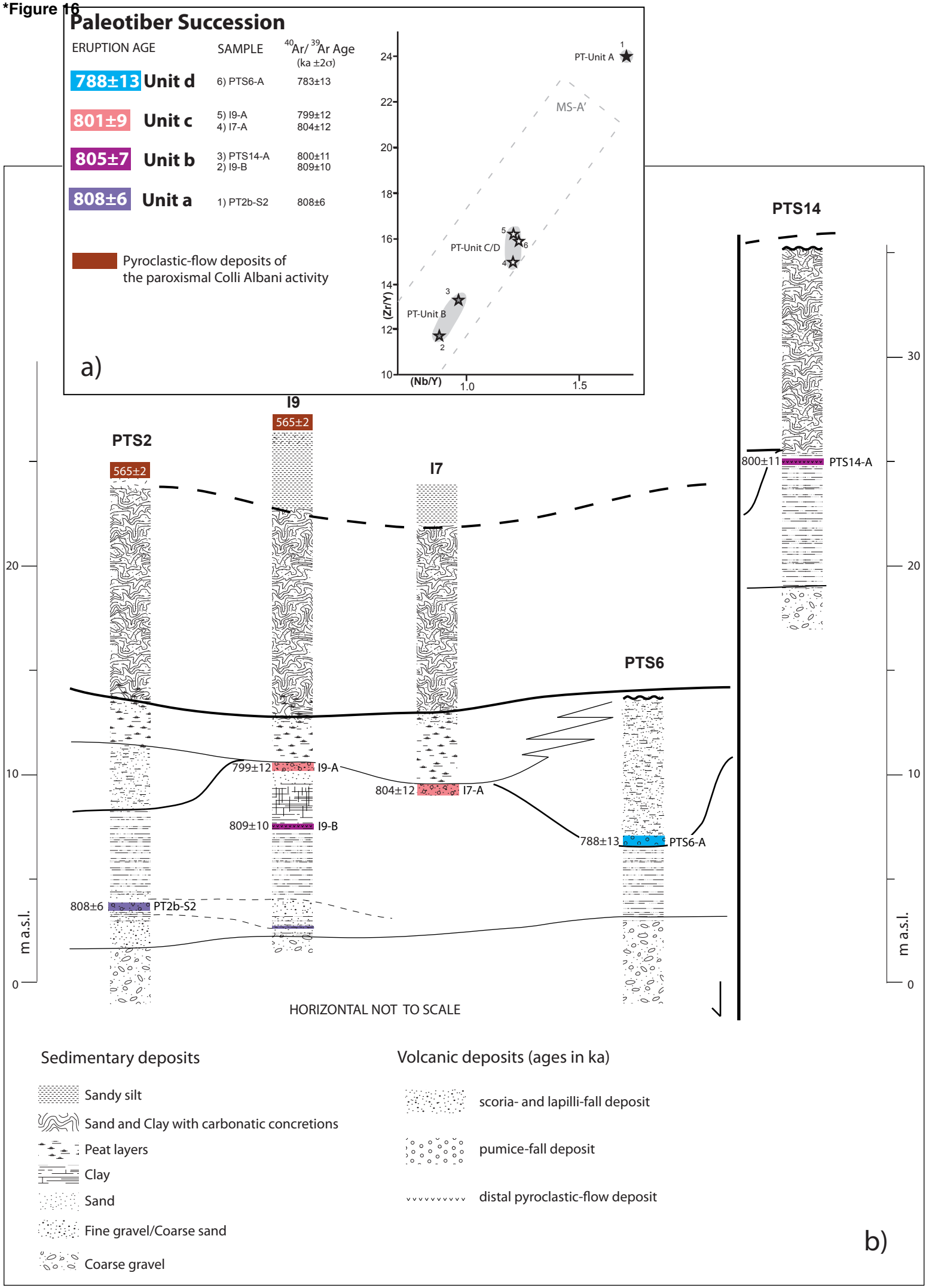

Figure 16

*Figure 17

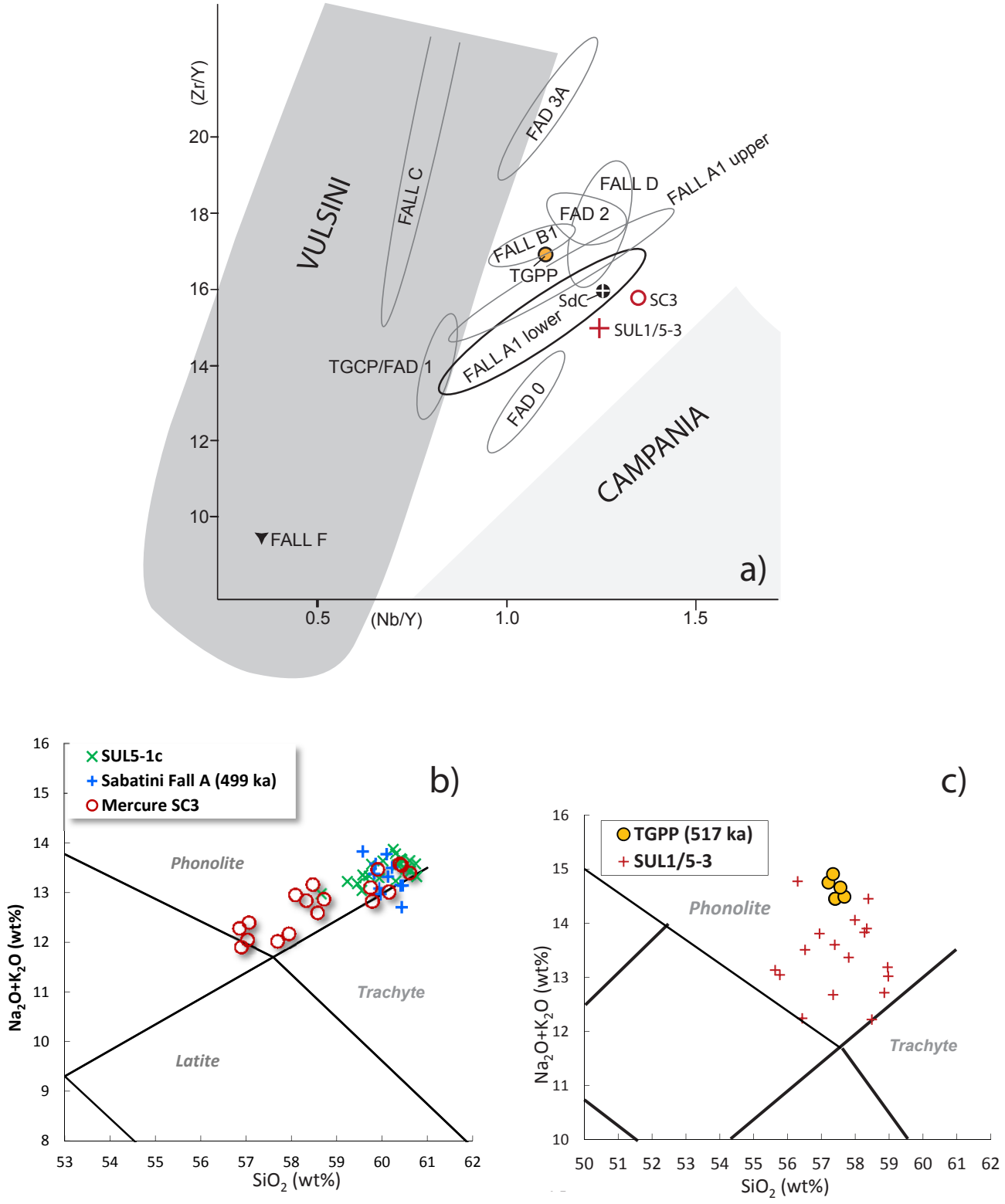

Figure 17

Supplementary Material #1

Click here to download Supplementary Data: Supplementary material #1.doc

Appendix 1

Click here to download Supplementary Data: Appendix 1.xls

Appendix 2

Click here to download Supplementary Data: Appendix 2.xls

Appendix 3

Click here to download Supplementary Data: Appendix 3.doc

Appendix 4

Click here to download Supplementary Data: APPENDIX 4.xls

Appendix 5

Click here to download Supplementary Data: Appendix 5.doc